Inorganic Chemistry

pubs.acs.org/IC
Article

Protoporphyrin IX-Derived Ruthenium(II) Complexes for Photodynamic Therapy in Gastric Cancer Cells

Andrés Restrepo-Acevedo, María Isabel Murillo, Christophe Orvain, Chloé Thibaudeau, Sevda Recberlik, Lucas Verget, Virginia Gómez Vidales, Christian Gaiddon, Georg Mellitzer,* and Ronan Le Lagadec*

Cite This: *Inorg. Chem.* 2025, 64, 9684–9702

Read Online

ACCESS | Metrics & More | Article Recommendations | Supporting Information

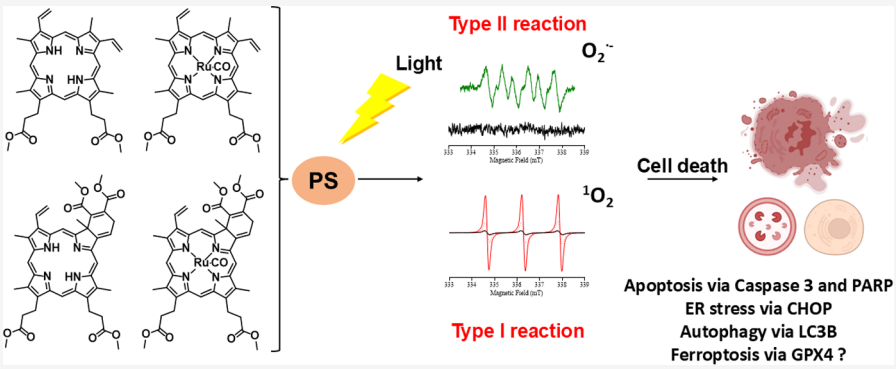

ABSTRACT: In recent years, photodynamic therapy (PDT) has emerged as a promising alternative to classical chemotherapy for treating cancer. PDT is based on a nontoxic prodrug called photosensitizer (PS) activated by light at the desired location. Upon irradiation, the PS reacts with the oxygen present in the tumor, producing cytotoxic reactive oxygen species (ROS). Compounds with highly conjugated π-bond systems, such as porphyrins and chlorins, have proven to be excellent light scavengers, and introducing a metal atom in their structure improved the generation of ROS. In this work, a series of tetrapyrrole-ruthenium(II) complexes derived from protoporphyrin IX and the commercial drug verteporfin were designed as photosensitizers for PDT. The complexes were almost nontoxic on human gastric cancer cells under dark conditions, revealing remarkable cytotoxicity upon irradiation with light. The ruthenium atom in the central cavity of the chlorin ligand allowed combined mechanisms in photodynamic therapy, as both singlet oxygen and superoxide radicals were detected. Additionally, one complex produced large amounts of singlet oxygen under hypoxic conditions. Biological assays demonstrated that the ruthenium derivatives caused cell death through a caspase 3 mediated apoptotic pathway and *via* CHOP, an endoplasmic reticulum stress-inducible transcription factor involved in apoptosis and growth arrest.

INTRODUCTION

Photodynamic therapy (PDT) is an approved anticancer strategy with high temporal selectivity, which presents several advantages over conventional radiotherapy and chemotherapy, such as few side effects and as a noninvasive therapy.[1,2] Platinum-based complexes, such as cisplatin, carboplatin, and oxaliplatin, have become the most used metal-based drugs worldwide for cancer treatment by chemotherapy.[3−5] However, although these anticancer drugs are very effective, their efficiency is limited due to the high incidence of resistance mechanisms. In addition, they lack selectivity toward cancer cells, which leads to numerous undesirable side effects such as nephrotoxicity, neurotoxicity, and ototoxicity, among others.[6,7] As an alternative to classical chemotherapy, PDT emerged as a promising strategy for treating cancer. Treatments by PDT are based on a nontoxic prodrug called a photosensitizer (PS) that can be activated by light at the desired location.[8,9] Upon photoactivation, the PS releases the energy needed to react with the oxygen present in the tumor, producing reactive oxygen species (ROS) such as singlet oxygen ($^1O_2$), superoxide radical ($O_2^{\bullet-}$), hydroxyl radical ($^{\bullet}OH$) and hydrogen peroxide (H_2O_2). Such species are spatially and temporally confined to the irradiated region, thus targeting malignant tissues without attacking healthy ones.[10] Two types of PDT have been described. In type II reaction, high amounts of highly toxic singlet oxygen are produced, causing oxidative damage in cells. In type I reaction, the PS in singlet or triplet excited state can react directly with a biological substrate and undergo hydrogen

Received: February 25, 2025
Revised: April 22, 2025
Accepted: April 28, 2025
Published: May 2, 2025

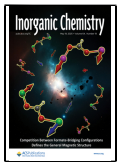

https://doi.org/10.1021/acs.inorgchem.5c00896
Inorg. Chem. 2025, 64, 9684−9702

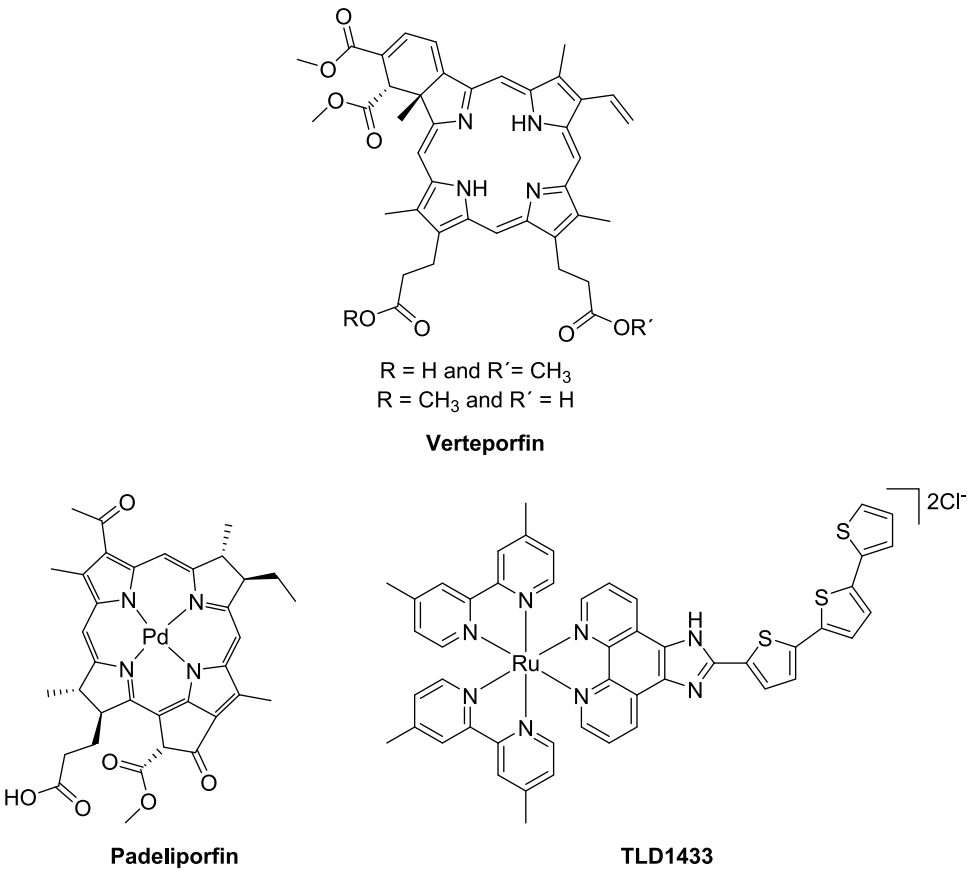

Figure 1. Compounds approved or in clinical trials as photosensitizers for PDT.

atom abstraction or electron transfer reactions, giving rise to highly reactive free radicals and radical ions, which can generate different ROS and cause cell death.[11−13]

Ideally, a PS should preferentially (i) accumulate in tumors, (ii) display no toxicity in the dark, and (iii) be rapidly eliminated from the body.[14,15] The PS should also present a high quantum yield of ROS production, a high molar extinction coefficient, and molar absorbance. Absorbance in the red spectral regions (600−800 nm) is desired for deep-seated tumors, *i.e.*, in cancers of the stomach, bladder, pancreas, esophageal or glioblastoma multiforme, among others.[14,16] Compounds with highly conjugated π-bond systems, such as porphyrins and chlorins, are excellent light scavengers and are, therefore, ideal PS for PDT.[17] Additionally, such tetrapyrrole structures can host a wide variety of metal ions. For example, it has been observed that metaloporphyrins with paramagnetic metal ions such as Cu(II) or Co(II) present low ROS production due to a decrease in the lifetime of the excited triplet state of the PS. On the contrary, metaloporphyrins with diamagnetic ions such as Zn(II), Pd(II), In(III), Ru(II), Ir(III), and Pt(II) present the heavy atom effect with a strong spin−orbital coupling that provides an absorbance lifetime long enough for the excited triplet state to interact with dioxygen, thus favoring the generation of ROS and, therefore, increasing the quantum yields.[13,18,19] For instance, a palladium(II) metalochlorin complex (padeliporfin, TOOKAD) has been approved in several EU countries, Israel and Mexico, for use as a PS for the treatment of localized prostate cancer (Figure 1).[20] Ruthenium(II) complexes have generated interest as photosensitizers in PDT due to their favorable photophysical properties compared to other transition metals, including broad absorption spectra and long excited state lifetimes. Moreover, the absorption and emission wavelengths can be precisely tuned through ligand design. Furthermore, ruthenium(II) complexes frequently exhibit high chemical and photochemical stability, allowing them to withstand light without degradation.[21,22] In this respect, TLD1433 (Figure 1) is the first ruthenium-based PS that has entered a phase II clinical trial to treat noninvasive bladder cancer.[23] Interestingly, in most of the reports where porphyrins and ruthenium are used, the metal atom is found in the peripheries of the macrocycle, and only a few metaloporphyrins with the ruthenium atom in the central cavity have been described.[24,25] However, many Ru(II) complexes are poorly soluble in water, which may limit their ability to reach target tissues. Low water solubility can cause aggregation, reduced bioavailability, and ineffective cellular uptake. The clinical applications of these complexes have also been restricted due to their cytotoxicity in the dark and low ROS generation efficiency.[21,26]

It is worth mentioning that PDT is not only used in cancer treatment. For instance, verteporfin (**VP**, Visudyne) is widely used for treating macular degeneration.[27] However, the use of **VP** has several disadvantages, such as high phototoxicity and slow elimination by the body, meaning that the patient will be photosensitized for more than 48 h after the therapy.[28,29]

Therefore, inspired by the photoproperties of porphyrins and chlorins, a ruthenium(II) ion was introduced in the central cavity of a series of tetrapyrroles to study their potential use as PS for the treatment of cancer, focusing on gastric cancer. Gastric cancer (GC) represents a public health problem due to its high aggressiveness, with a 5-year survival rate of less than

https://doi.org/10.1021/acs.inorgchem.5c00896
Inorg. Chem. 2025, 64, 9684−9702

Scheme 1. Synthesis of Ligands and Numbering Used for NMR Assignation

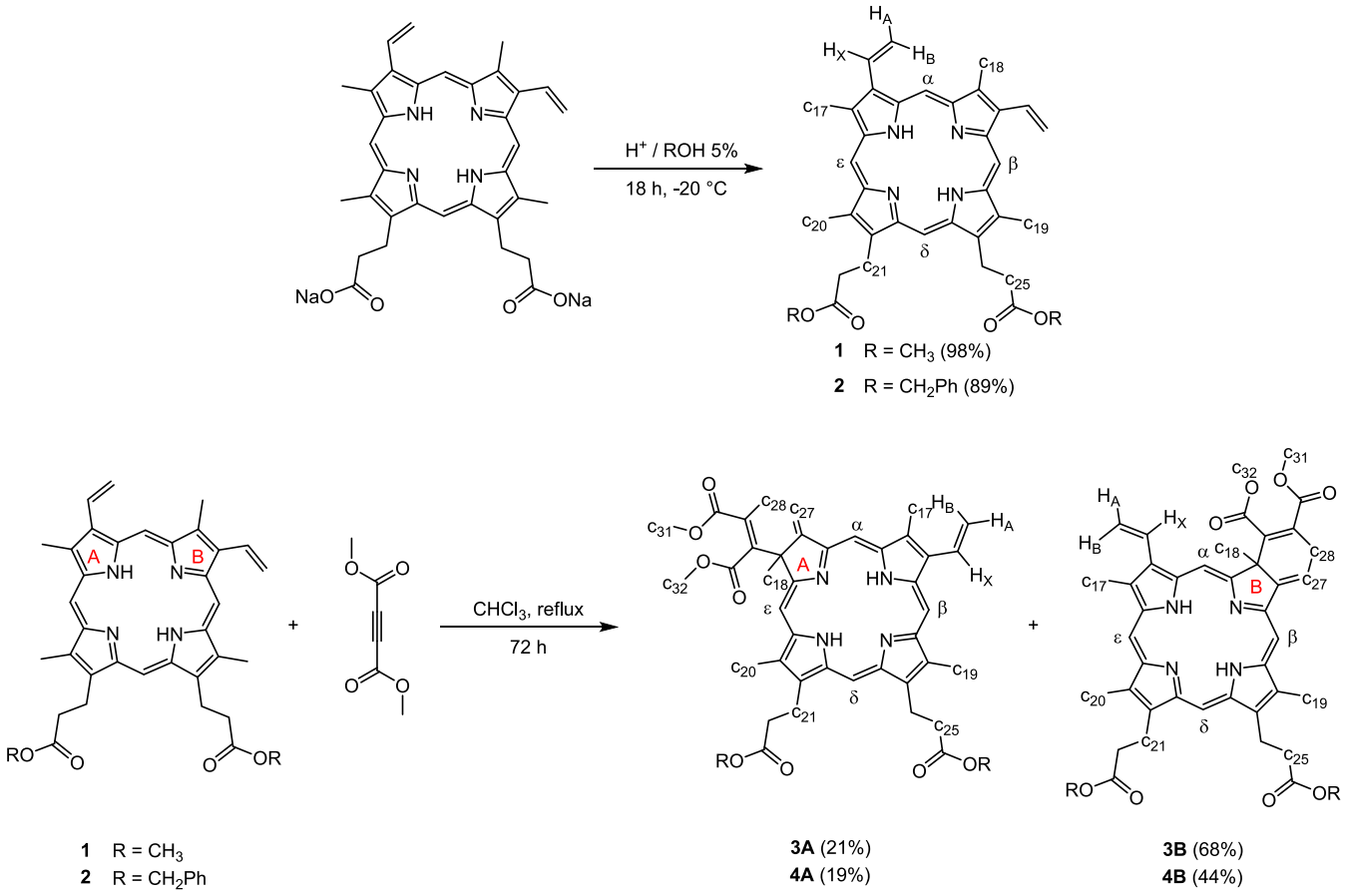

25% and a median survival of about 11 months. It represents the fifth leading cause of cancer-related death in the world, after lung, breast, colon, and liver cancers, with around 769,000 deaths in 2020 (7.7% of all cancers), according to the World Health Organization (WHO).[30] In terms of incidence, GC is the fifth most common cancer, with more than one million new cases diagnosed in 2020 (5.6% of all cancers).[31,32] Treatment options are still very limited, and patient management is mainly based on partial or complete gastrectomy combined with oxaliplatin-based (oxaliplatin + 5-Fluorouracyl) neoadjuvant and/or adjuvant chemotherapy. Unfortunately, the efficacy of the treatment is impaired by various resistance mechanisms,[33] notably due to mutation in p53, which is mutated in up to 70% of GC.[34] Consequently, there is an urgent need to develop new therapeutic solutions whose mode of action is independent of p53. In this respect, ruthenium-based anticancer compounds have been shown to induce cell death independently of p53, targeting different metabolic pathways and reducing tumor growth *in vivo*.[35−37] In addition, as the gastric cavity is accessible by endoscopy, combining ruthenium with PDT would be an attractive solution for a localized GC treatment.

RESULTS AND DISCUSSION

Chemistry. *Synthesis and Characterization.* The porphyrins **1** and **2** derived from protoporphyrin IX (**PpIX**) were synthesized by adapting a described procedure from commercial **Na_2PpIX** salt and methanol or benzyl alcohol in an acidic medium (Scheme 1).[38]

Porphyrins **1** or **2** were used to prepare the chlorins through a Diels−Alder reaction, modifying a reported procedure.[39,40] Porphyrin **1** or **2** was refluxed with dimethyl acetylenedicarboxylate (DMAD) in dry chloroform for 72 h to form mixtures of **3A** and **3B**, or **4A** and **4B** chlorins (Scheme 1). Isomers **A** and **B** were readily separated by column chromatography on silica gel and characterized by one-dimensional (1D) and two-dimensional (2D)-NMR techniques.

The **1** and **2** porphyrins and **3A** and **3B** chlorins were used as ligands to react with $[Ru_3(CO)_{12}]$ to form the new ruthenium(II) complexes. Scheme 2 summarizes the synthesis of the ruthenium derivatives. Two strategies were used to synthesize ruthenium complexes based on chlorins. In the first approach, a mixture of chlorins **AB** was reacted with $[Ru_3(CO)_{12}]$, followed by chromatographic separation of the resulting ruthenium complexes. However, the reaction yield was low, and the separation of the isomers was problematic. Therefore, the second methodology consisted of starting from the purified **3A** or **3B** isomers. Ruthenium complexes were obtained in 13 and 16% yields from the isolated isomer, respectively. The **4A** and **4B** ligands were not metalated as they were obtained in very low quantities. All the new ruthenium(II) derivatives are stable in air and light in the solid state and solution.

All the new compounds were characterized by IR, HR-MS, ^{1}H and ^{13}C NMR, DEPT-135, HSQC, and HMBC, and their purity was confirmed by HPLC (Figures S1−S61). In addition, crystals suitable for single-crystal X-ray diffraction crystallography were obtained for **Ru-1** and **3B**.

https://doi.org/10.1021/acs.inorgchem.5c00896
Inorg. Chem. 2025, 64, 9684−9702

Scheme 2. Synthesis of Ruthenium Complexes and Numbering Used for NMR Assignation

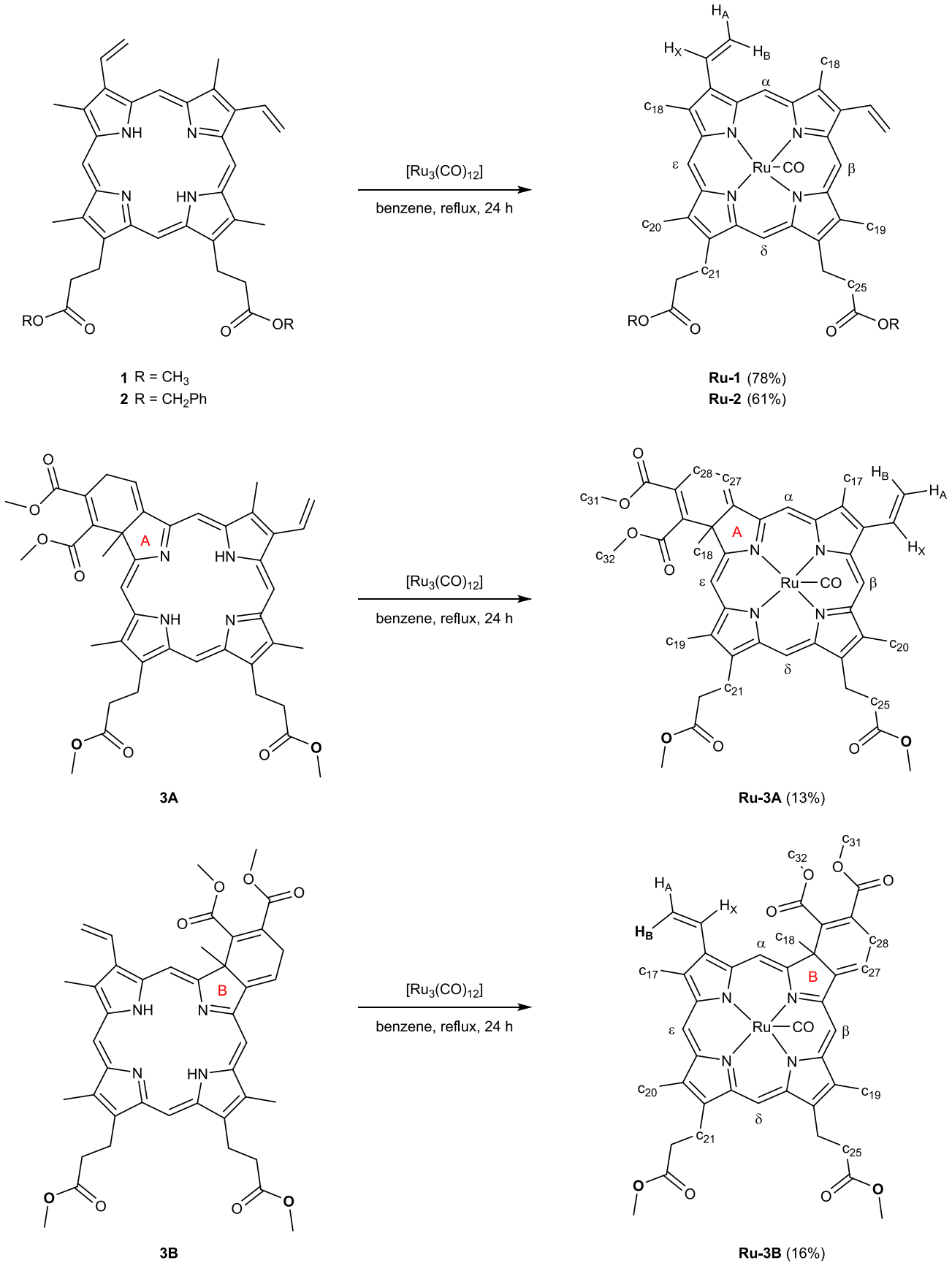

https://doi.org/10.1021/acs.inorgchem.5c00896
Inorg. Chem. 2025, 64, 9684−9702

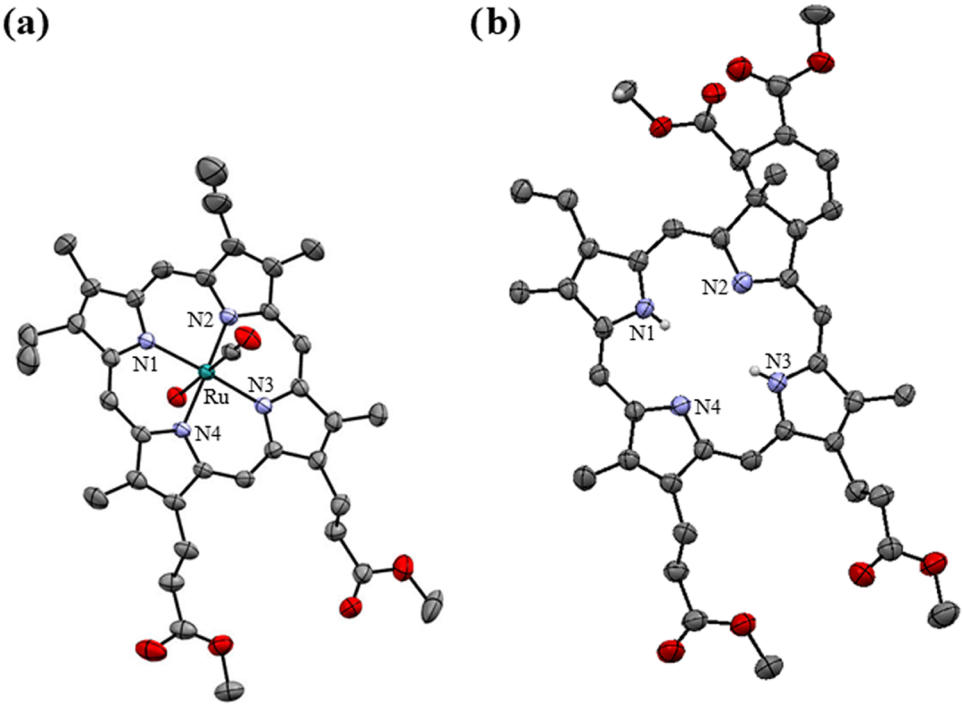

Figure 2. ORTEP diagrams (a) **Ru-1** and (b) **3B**. Thermal ellipsoids are drawn with a 40% probability level. Hydrogen atoms are omitted for clarity, except for N−H hydrogen atoms.

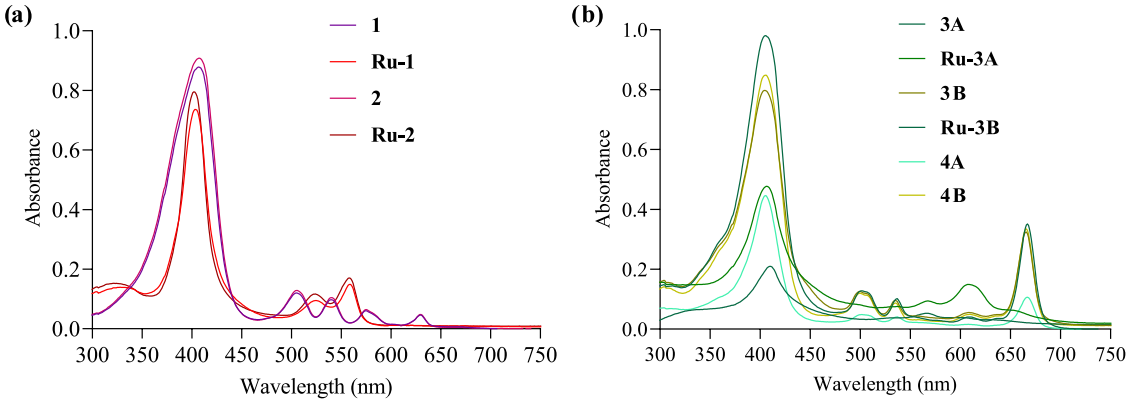

Figure 3. Absorption spectra of (a) porphyrins and metaloporphyrins and (b) chlorins and metalochlorins in DMSO, 1×10^{-5} M at 37 °C.

Crystallography. **Ru-1** and **3B** crystals were obtained by slow evaporation of a hexane/dichloromethane solution. Figure 2 shows the ORTEP diagrams of the structures, and crystallographic data are summarized in Table S1.

Compound **3B** crystallized in an orthorhombic system with space group *Fdd2*, and the structure confirms the cycloaddition. The bond distance between N−H1 and N−H2 is 0.737 and 0.701 Å, respectively. In addition, it is observed that the central structure of the chlorin is planar. **Ru-1** complex crystallized with a water molecule (probably from the solvents used for crystallization) in the *C*2/*c* space group. It has been reported that in similar porphyrin complexes, water, methanol, and ethanol molecules can weakly bind to the metal center *trans* to the CO ligand.[41,42] The angle between the H_2O−Ru−C(O) atoms is 179.04°, while the angles between the nitrogen atoms of porphyrin and ruthenium atom are 173.72 and 173.83°, indicating that the structure exhibits a slightly distorted octahedral geometry. The bond distances between Ru-CO and Ru−OH_2 are 1.782(5) and 2.224(4) Å, respectively. The bond distances between Ru−N1, Ru−N2, Ru−N3, and Ru−N4 are 2.051, 2.057, 2.050, and 2.059 Å, respectively.

Electronic Absorption. The ultraviolet−visible (UV−vis) absorption spectra of the ligands and complexes were measured in dimethyl sulfoxide (DMSO) at 37 °C at a 1×10^{-5} M. Figure 3 shows the spectra for the ligands and complexes, and electronic absorption data are given in Table S2.

A strong Soret absorption band around 400 nm is observed in all the UV−vis spectra, indicating π−π^* transitions (Figure 3).[43] For the ligands, four Q bands in the visible region are attributed to an π-π^* electronic transition ($a_{1u} \rightarrow e_g^*$) arising from the ground state (S_0) to the second excited state (S_2).[44] For the metaloporphyrinoid derivatives, the bands around 500 to 600 nm are assigned to charge transfer transitions, π-dπ between the tetrapyrrole ring and the metal. In the complexes, the decrease in the number of Q bands is ascribed to a change

https://doi.org/10.1021/acs.inorgchem.5c00896
Inorg. Chem. 2025, 64, 9684−9702

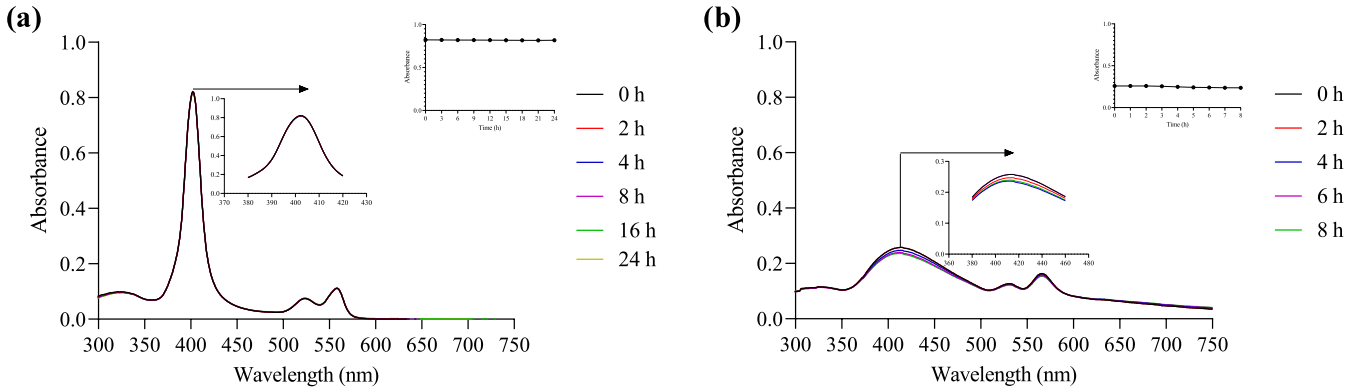

Figure 4. Stability assay for **Ru-1** in (a) DMSO and (b) PBS/DMSO 0.1%. Inset: plot of absorbance *vs* time.

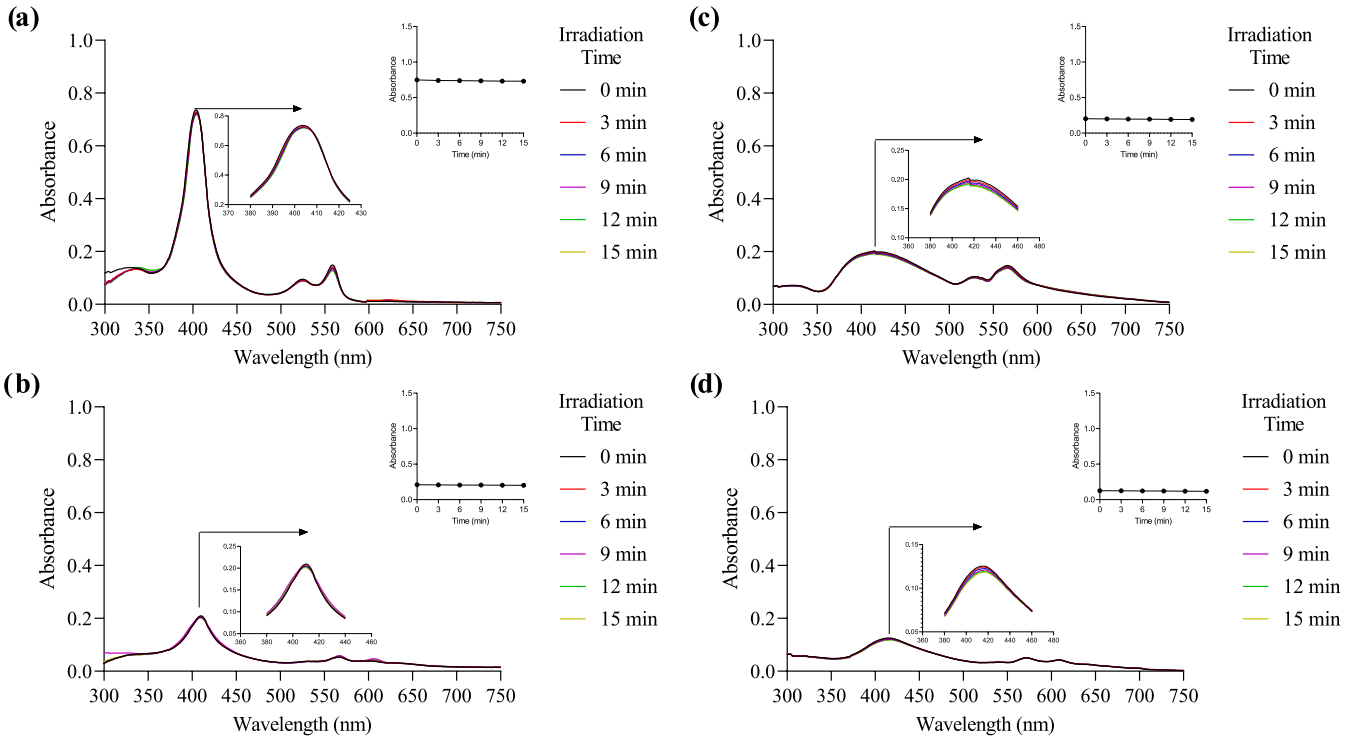

Figure 5. Photodegradation of compound **Ru-1** (a, c) and **Ru-3B** (b, d) in DMSO and PBS/DMSO (0.1%) upon irradiation with white light (50% intensity of a 12 W lamp). Inset: plot of absorbance *vs* time.

in the symmetry, from D_2h to D_4h, due to the deprotonation and cation formation.[43,44]

Stability. The stability of the compounds was evaluated by UV−vis spectroscopy. Figures S62−S70 show the absorption spectra of each compound in DMSO for 24 h at 37 °C at a concentration of 1×10^{-5} M. The stability was also evaluated in PBS containing 0.1% DMSO (1×10^{-5} M) at 37 °C for 8 h. In DMSO, practically no decomposition of the compounds was observed (Figure 4a). However, in PBS/DMSO (0.1%), a slight decomposition was noted (between 1−10%), as seen in Figure 4b. Figures S71−S79 show the absorption spectra of each compound in PBS/DMSO (0.1%). However, in the case of compound **Ru-2**, the decomposition was more important (48% in PBS/DMSO), as observed in Figure S73.

Photobleaching. Degradation of the molecules upon light irradiation can cause problems in applications such as photodynamic therapy.[45] Photodegradation is an oxidative degradation of a molecule over time into fragments of lower molecular weight, implicating that the molecule may lose its photodynamic activity during irradiation.[46,47]

The measurement of light tolerance and stability of each compound was studied by UV−vis spectroscopy at 37 °C at 1×10^{-5} M. The cell was irradiated with white light, and a spectrum was recorded every 3 min until a total of 5 measurements (15 min). Figure 5 shows the spectra obtained during **Ru-1** and **Ru-3B** photobleaching in pure DMSO (Figure 5a) and PBS/DMSO (0.1%) (Figure 5b). Spectra for the remaining compounds are shown in Figures S80−S87. In all cases, only a slight decrease (1−5%) in the absorption of the Soret band (404−410 nm) was observed.

Fluorescence and Singlet Oxygen Formation Quantum Yield Measurements. Emission spectra were measured in DMSO. The free ligands were excited at 503 nm, while the ruthenium complexes were excited at 573 nm. The spectra are shown in Figures S88−S93. For the calculation of fluorescence quantum yield, verteporfin (Φ_f = 0.0085) was used as a

https://doi.org/10.1021/acs.inorgchem.5c00896
Inorg. Chem. 2025, 64, 9684−9702

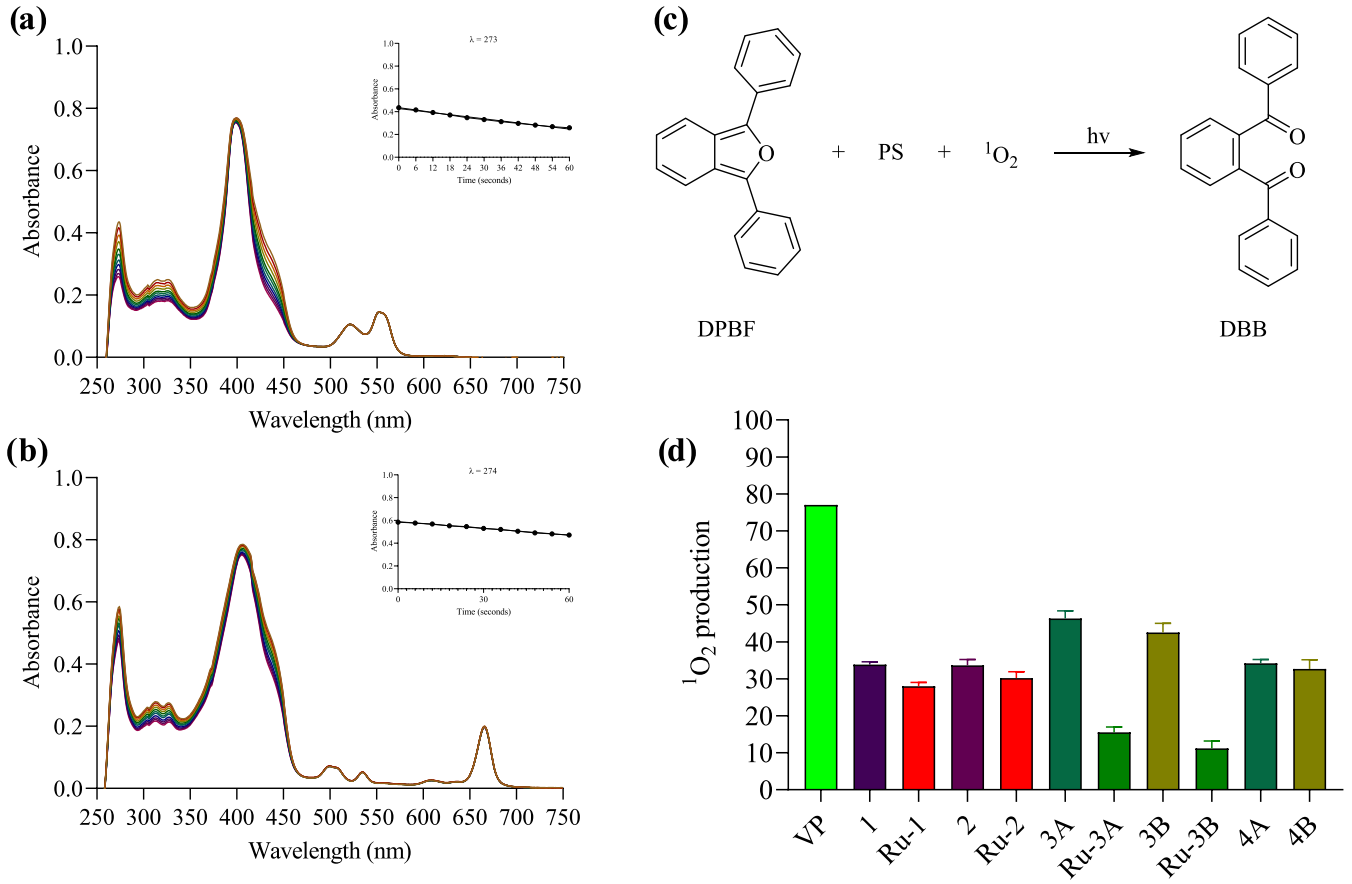

Figure 6. Absorption changes during the determination of singlet oxygen quantum yield of **Ru-1** (a) and **3B** (b) using DPBF as singlet oxygen trapping in DMSO equilibrated with air (inset: plot of absorbance at 214 nm *vs* irradiation time). (c) Reaction between DPBF and photosensitizer in the presence of light and oxygen. (d) Percentage singlet oxygen formation quantum yield relative to verteporfin (Φ_Δ = 0.77[46]). [PS] = 7×10^{-6} M; [DPBF] = 2×10^{-5} M, N = 3.

reference.[46] The results are shown in Table S2. In all metal-free compounds, an intense emission band at approximately 630–670 nm and a small band at approximately 700–750 nm were observed, assigned to Q (0–0) and Q (1–0) transitions, respectively.[48] On the other hand, the new ruthenium(II) complexes showed no emission. A similar behavior has been observed in palladium(II) and nickel(II) metaloporphyrins, where the fluorescence was quenched due to electron or energy transfer.[49]

An indirect method was used to calculate the singlet oxygen production quantum yield of all compounds using 1,3-diphenylisobenzofuran (DPBF), which in the presence of $^1O_2$ oxidizes to 1,2-dibenzoylbenzene (DBB) (Figure 6c). Verteporfin was selected as a reference (Φ_Δ = 0.77 in DMSO).[46] The spectral change of the absorbance band at 214 nm of the DPBF scavenger was monitored to determine the singlet oxygen generation. Eleven measurements were made in a spectrophotometer, one measurement every 6 s after irradiating the samples with white light, for a total of 60 s. Figure 6d summarizes the data obtained.

In all cases, the absorbance of DPBF at 214 nm decreased in the presence of the compounds, confirming the generation of singlet oxygen. All the compounds, but **Ru-3A** and **Ru-3B**, were highly efficient in generating singlet oxygen, with quantum yields between 30 and 50%. Interestingly, for **Ru-3A** and **Ru-3B**, the singlet oxygen quantum yields were much lower (15% and 11%, respectively) than for the corresponding free ligands (**3A** and **3B**) and the other ruthenium complexes (Figure 6d).

Determination of ROS Production. Since singlet oxygen has a very short half-life, a spin trap and detection of the generated radical by electron paramagnetic resonance (EPR) were used as an indirect method to monitor its formation. The spin trap of choice was 2,2,6,6-tetramethylpiperidine (TEMP), as it can readily be converted into the stable radical 2,2,6,6-tetramethyl-1-piperidinyloxy (TEMPO) in the presence of singlet oxygen. The formation of TEMPO was monitored by continuous white light irradiation of the PS *in situ* for 15 min. As seen in Figure 7a–d, the characteristic triplet signal (g = 2.0063 and hfcc = 1.63 mT) for TEMPO was detected for all compounds. However, as previously observed, the production of $^1O_2$ by the metalochlorins **Ru-3A** and **Ru-3B** was much lower (Figure 7e).

Because our compounds were producing $^1O_2$ under normal conditions, the effect of the oxygen concentration in the samples was evaluated. Compounds **1**, **Ru-1**, **3B**, and **Ru-3B** were selected for this experiment. Interestingly, compound **Ru-1** produced significant amounts of $^1O_2$ at low oxygen concentrations, which might indicate that it could potentially be active in type II PDT on hypoxic cancer cells.[50] Figure 8 shows the EPR spectra obtained at different O_2 concentrations for **Ru-1**, and the spectra for compounds **1**, **3B**, and **Ru-3B** are shown in Figures S94–S96, respectively.

https://doi.org/10.1021/acs.inorgchem.5c00896
Inorg. Chem. 2025, 64, 9684–9702

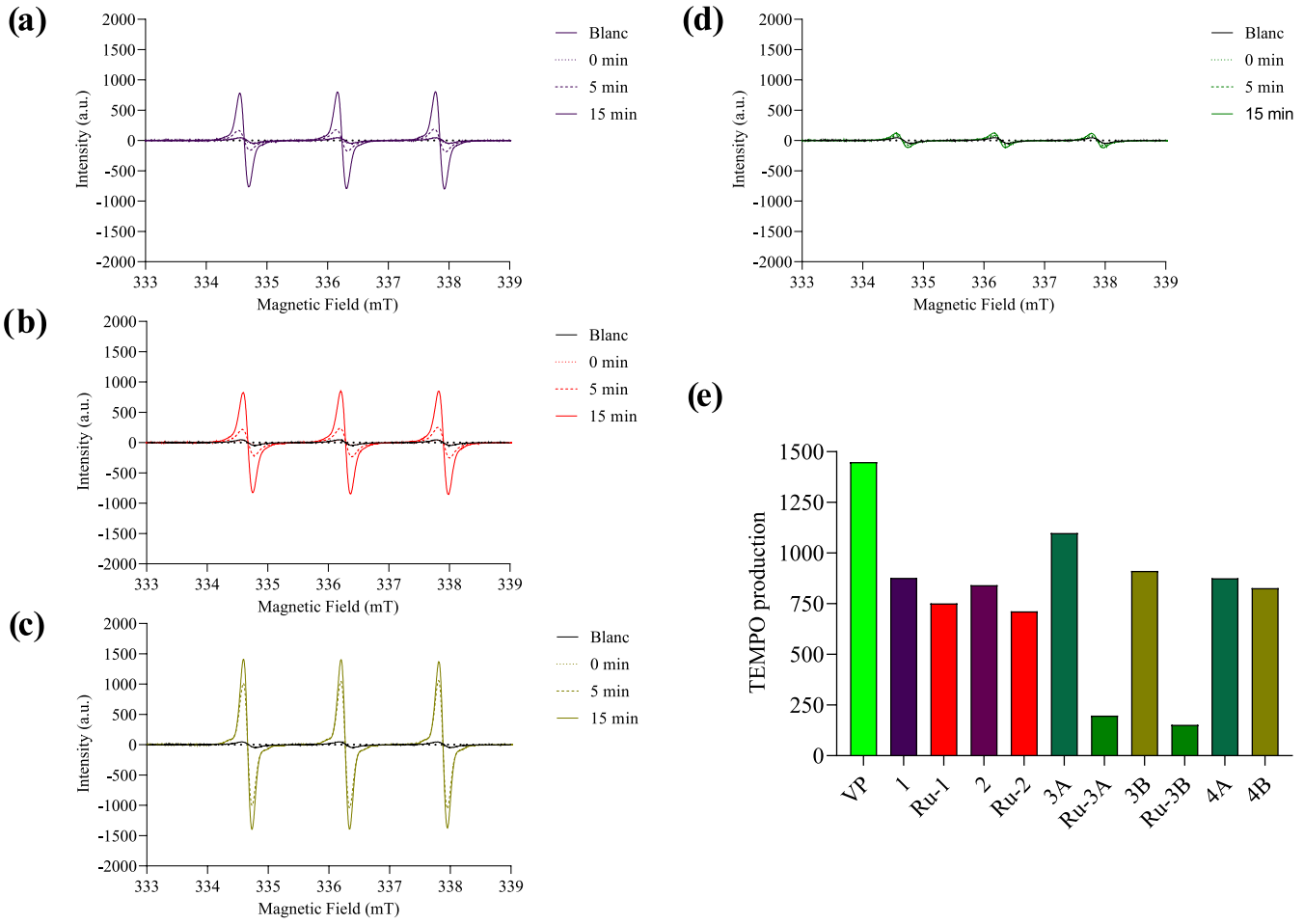

Figure 7. EPR spectra upon irradiation with white light of the PS in the presence of TEMP spin trap in ethanol/DMSO at room temperature: (a) **1**, (b) **Ru-1**, (c) **3B**, and (d) **Ru-3B**. (e) TEMPO signal intensity after 15 min of irradiation. [PS] = 1×10^{-3} M, [TEMP] = 4×10^{-3} M, blanc = spectra of TEMP without PS.

Contemplating that type I PDT can also occur when the PS is irradiated, the possibility that the metalochlorins **Ru-3A** and **Ru-3B** can generate ROS different from $^1O_2$ was investigated. Therefore, another spin trap, 5,5-dimethyl-1-pyrroline-*N*-oxide (DMPO), able to react with superoxide radical $O_2^{\bullet-}$ was used. Figure 9a–c show the EPR spectra obtained in the presence of DMPO before and after irradiation with white light for 15 min. As expected, no ROS is produced without the PS (Figure 9a). When the sample containing the PS (**Ru-3A** or **Ru-3B**) and DMPO was irradiated with white light for 15 min, the characteristic signal and coupling constants for the DMPO-$^{-}O_2^{\bullet-}$ adduct (g = 2.0060, hfcc = 1.330 mT) were observed (Figure 9b,c).[51,52] Such results confirm that our metalochlorins can exhibit combined mechanisms of action for PDT, *i.e.*, they can produce singlet oxygen in the type II mechanism, as well as the superoxide radical in a type I mechanism. The Soret band of **Ru-3A** and **Ru-3B** metalochlorins showed a lower absorption intensity than for ligands **1**, **2**, **3A**, and **3B**, and complexes **Ru-1** and **Ru-2**. A higher Soret band absorption intensity usually indicates a larger gap between the highest occupied molecular orbital (HOMO) and lowest unoccupied molecular orbital (LUMO), while a lower Soret band absorption intensity means a smaller HOMO–LUMO gap.[53,54] According to the literature, a small HOMO–LUMO gap facilitates the intermolecular transfer of photo-induced electrons from the excited triplet state to the ground state to produce the superoxide radical, as observed in our study.[55] However, theoretical calculations in the excited states are necessary to fully explain why the metalochlorins specifically produce superoxide radicals.

Lipophilicity. The *n*-octanol/water partition coefficient ($\log P_{o/w}$) is a well-established parameter that helps to predict the biological activity of drugs and other biologically active compounds.[56] The so-called "shake-flask" method was adopted to determine the partition coefficient using 1-octanol and PBS (phosphate-buffered saline) as solvents.[57] The results are summarized in Table 1. All the porphyrin derivatives presented low lipophilicity values. At the same time, the chlorin compounds were much more lipophilic as expected due to the reduction of one of the pyrrole rings and the formation of the new ring in the chlorin.

Biological Assays. *Impact of Porphyrins, Chlorins, and Ru(II) Compounds on Gastric Cancer Cell Survival.* To assess the anticancer potential of compounds, the cytotoxicity was evaluated on the gastric cancer cell line AGS. The cells were treated in the dark for 8 h with increasing concentrations of the different compounds (Table 2). Cisplatin was used as a positive cytotoxic and clinically used drug control, and verteporfin (**VP**) or protoporphyrin-IX (**PpIX**) were used as positive PDT controls. Cells were then irradiated for 15 min with white light or kept in the dark and further cultivated for 48h in the dark. An MTT test was then performed to evaluate

https://doi.org/10.1021/acs.inorgchem.5c00896
Inorg. Chem. 2025, 64, 9684–9702

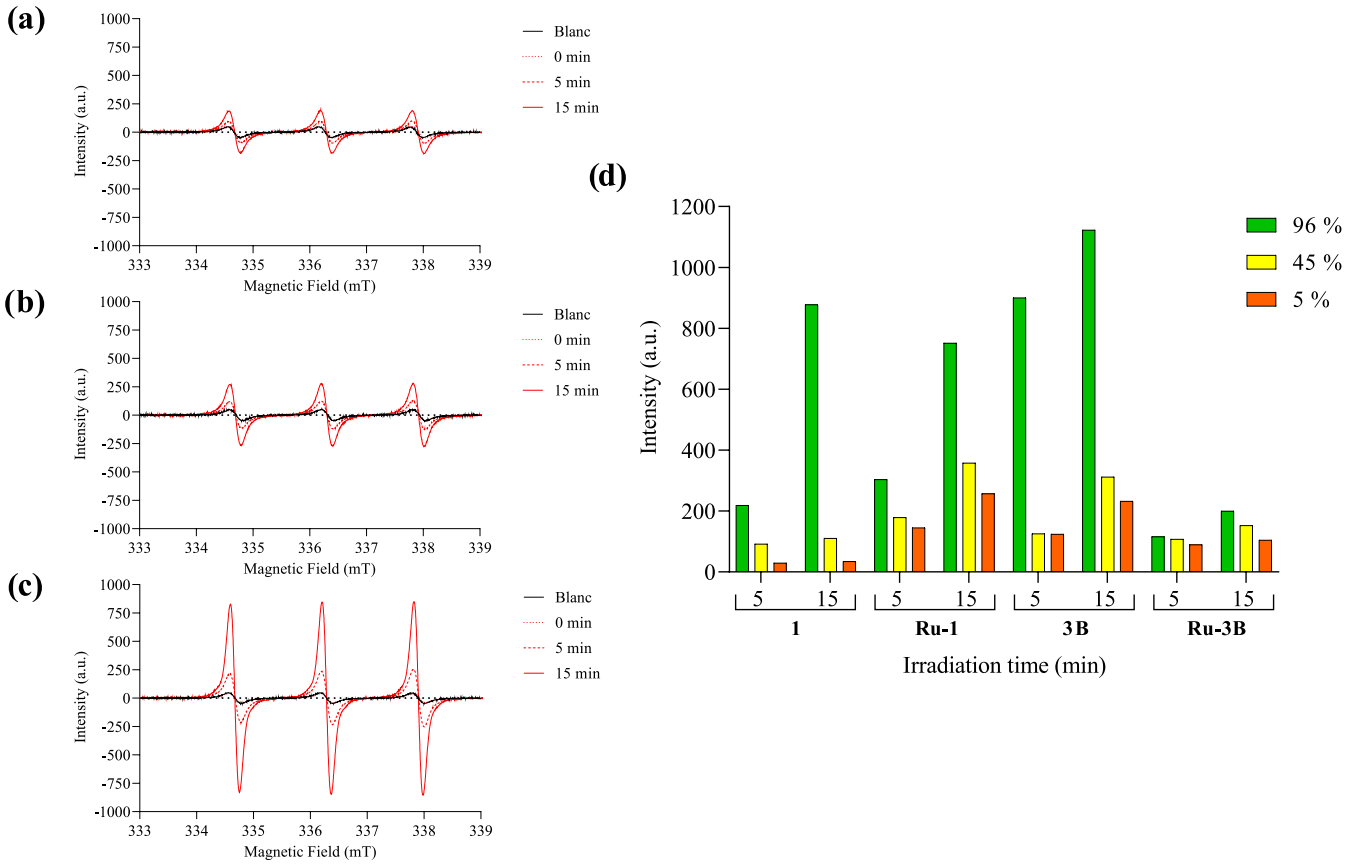

Figure 8. EPR spectra upon irradiation for 5 and 15 min of **Ru-1** in the presence of TEMP varying the oxygen concentration: (a) 5% of oxygen, (b) 45% of oxygen, (c) 96% of oxygen. (d) TEMPO signal intensity for compounds **1**, **Ru-1**, **3B**, and **Ru-3B** at 15 min of irradiation at different oxygen concentrations. [PS] = 1×10^{-3} M, [TEMP] = 4×10^{-3} M, blanc = spectra of TEMP without PS.

the impact of the different treatments on cell survival. This demonstrated that in the dark, and, in contrast to cisplatin (IC_{50} = 29 μM) and verteporfin (IC_{50} = 7 μM), all compounds displayed very low toxicity on AGS cells, with an IC_{50} which could not be calculated, except for **Ru-1** (IC_{50} = 95 μM) and **Ru-3A** (IC_{50} = 64 μM) (Table 2, Figures 10, and S97−S101). After irradiation, all compounds showed a marked increase in their toxicity, ranging between 0.1 and 4 μM, which, except for **Ru-2** (IC_{50} = 51 μM), were below the IC_{50} of cisplatin (Figure 10 and Table 2). The difference in the observed toxicity is most likely not due to a difference in cellular uptake, as there does not appear to be a correlation between their lipophilicity and the IC_{50} values. The lower cytotoxicity of **Ru-2** is most likely due to its low stability in biological media, as determined by stability tests in PBS/DMSO. The phototoxicity index (PI) was calculated based on the IC_{50} dark/light ratio, and values as high as 1000 and 555 were calculated for compounds **3A** and **3B**, respectively.[58]

Given these results, compounds **1**, **Ru-1**, **3B**, and **Ru-3B** were selected as lead compounds for further studies. **Ru-3B** complex is of special interest as it could present different PDT mechanisms, combining the production of $^1O_2$ by the type II mechanism and $O_2^{\bullet-}$ radicals by a type I mechanism (as mentioned above). This capacity might be of significant importance for the design of new PS since the production of $O_2^{\bullet-}$ radicals does not directly depend on the concentration of oxygen present in the hypoxic microenvironment of cancer cells.[59−61]

Induction of Cell Deaths by Porphyrins, Chlorins, and Ruthenium Compounds. The therapeutic effects of PDT treatment on cancer cells are thought to be mainly related to ROS production, which are highly reactive and cytotoxic species that can induce cell death by apoptosis.[62] It has also been shown that ruthenium compounds can induce different cell death pathways.[63,64] For these reasons, we initially analyzed by Western blot the expression of cleaved caspase 3 and PARP, which are two well-known markers for programmed cell death apoptosis.[65−70] For this, AGS cells were treated at the IC_{50} of each compound for 4 h in the dark and then irradiated, or not, with white light for 15 min. The cells were then further cultivated in the dark for 24 h. Figure 11 shows that, except for **PpIX**, all compounds induced the cleavage of caspase 3 and PARP after irradiation, notably compound **1**, which was as efficient as **VP**. Then, the protein expression of CHOP, a key component of the endoplasmic reticulum (ER) stress-mediated apoptosis pathway and known to be induced by ruthenium compounds, was evaluated.[71,72] All compounds, except for **PpIX**, induced the expression of CHOP upon irradiation. Interestingly, CHOP expression was much more strongly induced by the ruthenium compounds compared to their respective free ligands or verteporfin, suggesting that they possibly lead to a much stronger accumulation of misfolded or unfolded proteins and/or ROS production (Figure 11).[73,74] Furthermore, CHOP has been reported to participate in the regulation of ER stress-mediated autophagy.[75−77] Autophagy is a cellular self-degradation system that facilitates the degradation of damaged organelles and

https://doi.org/10.1021/acs.inorgchem.5c00896
Inorg. Chem. 2025, 64, 9684−9702

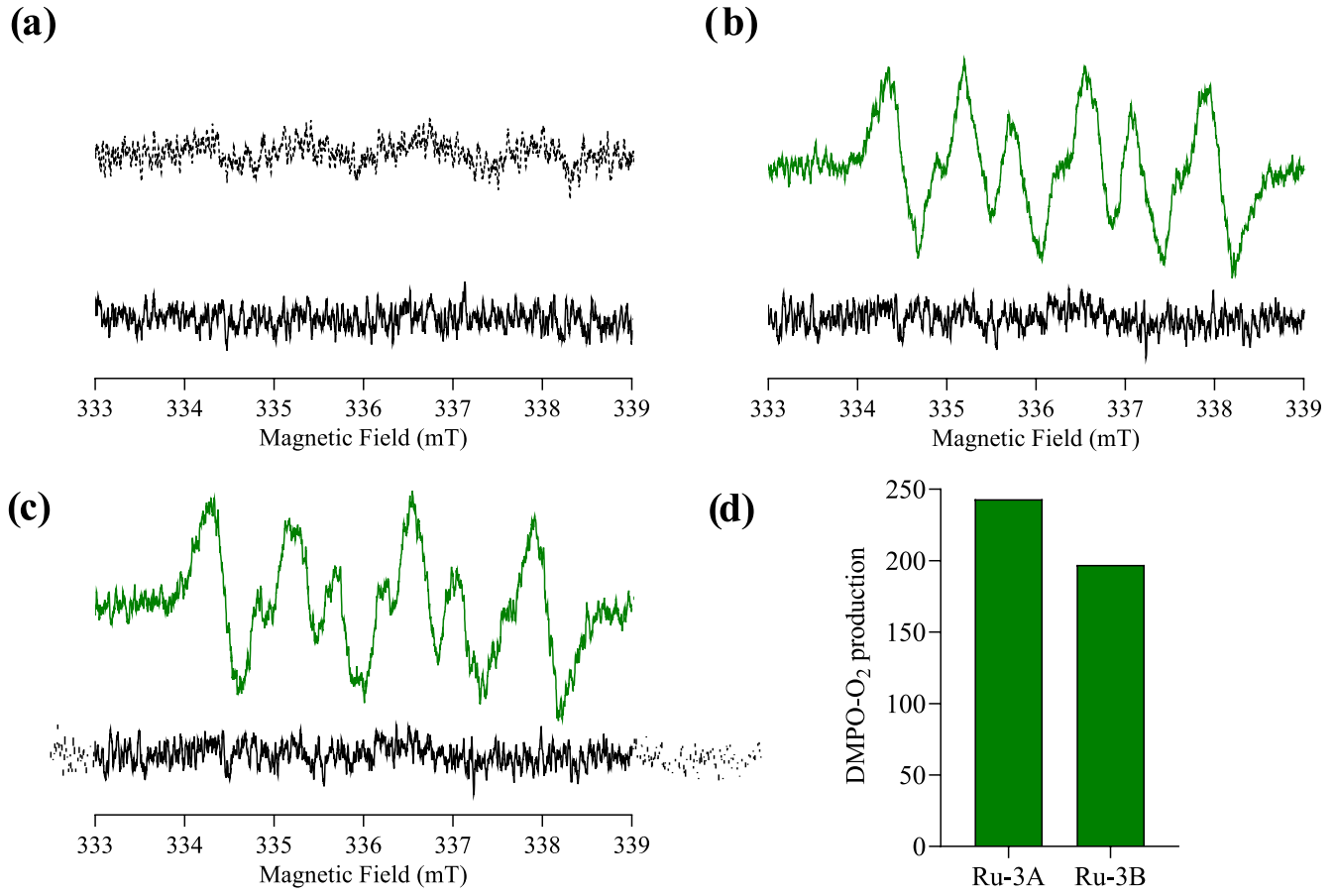

Figure 9. EPR spectra in methanol/DMSO at room temperature: (a) DMPO in the dark (solid line) and upon irradiation (dotted line), (b) **Ru-3A** in the dark (black) and upon irradiation (green), and (c) **Ru-3B** dark (black) and upon irradiation (green). (d) DMPO- $O_2^{\bullet-}$signal intensity after 15 min of irradiation. [PS] = 1×10^{-3} M, [DMPO] = 0.07 M. Irradiation time = 15 min.

Table 1. Partition Coefficient ($\log P_{o/PBS}$) of Compounds[a]

compound	$\log P_{O/PBS}$
1	0.957 ± 0.056
Ru-1	1.014 ± 0.058
2	1.063 ± 0.142
Ru-2	1.032 ± 0.108
3A	1.478 ± 0.083
Ru-3A	1.396 ± 0.051
3B	1.661 ± 0.088
Ru-3B	1.510 ± 0.177
4A	1.368 ± 0.042
4B	1.682 ± 0.176
VP	1.374 ± 0.064

[a]The value obtained is the average of three independent experiments at 27 °C.

Table 2. Mean Inhibitory Concentrations (IC_{50}) of the Compounds in AGS Gastric Cancer Cells[a]

	IC_{50} (μM)		
compound	light	dark	PI
cisplatin		29	
PpIX	0.5	>100	>200
Vp	0.003	7	=13,270
1	1.7 ± 0.184	>100	>17
Ru-1	3.8 ± 0.379	95 ± 0.462	=25
2	2.6 ± 0.100	>100	>18
Ru-2	51.3 ± 1.249	>100	>2
3A	0.1 ± 0.06	>100	>1000
Ru-3A	1.7 ± 0.100	64.1 ± 0.815	=38
3B	0.2 ± 0.021	>100	>555
Ru-3B	3.2 ± 0.252	>100	>31
4A	2.5 ± 0.231	>100	>40
4B	2.8 ± 0.265	>100	>36

[a]Cells were incubated for 8 h, followed by irradiation with white light for 15 min or kept in dark condition. The MTT assay was performed to determine cell viability after 48 h of treatment. $N = 3$.

misfolded or mutant proteins.[78] In cancer, autophagy protects tumor cells during cancer progression. However, it can also suppress cancer cell development or induce cell death.[79,80] Autophagy is characterized by the formation of autophagosomes, which express LC3B proteins. To investigate this, the expression and conversion of LC3B−I to LC3B−II was analyzed by Western blot (Figure 11). The results show that following irradiation, all ruthenium compounds induced the expression of LC3B−I and LC3B−II (Figure 11). Interestingly, upon light activation, **3B** and **Ru-3B** led to a marked induction of LC3B−I/II expression, similar to verteporfin, suggesting a specific induction of autophagy (Figures 11 and S102)

Ferroptosis, another form of nonapoptotic cell death, can promote inflammation and is triggered by iron-catalyzed lipid peroxidation *via* Fenton-type reactions, where the main ROS responsible for lipid damage are hydroxyl radical and

https://doi.org/10.1021/acs.inorgchem.5c00896
Inorg. Chem. 2025, 64, 9684−9702

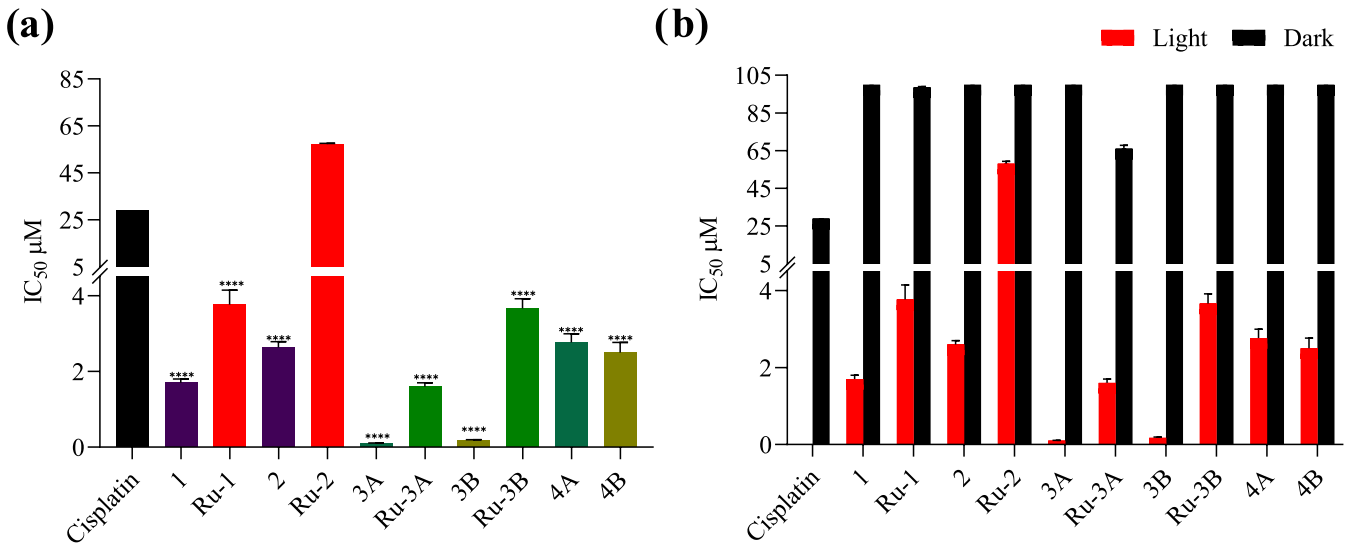

Figure 10. (a) Graphs showing the mean IC_{50} inhibitory concentrations presented in Table 2. Student's *t*-test is considered significant at $p < 0.5$. * < 0.05, ** < 0.01, *** < 0.001, **** < 0.0001 with respect to cisplatin. (b) Comparison of the minimum inhibitory concentration in the dark and activated under irradiation with white light for 15 min.

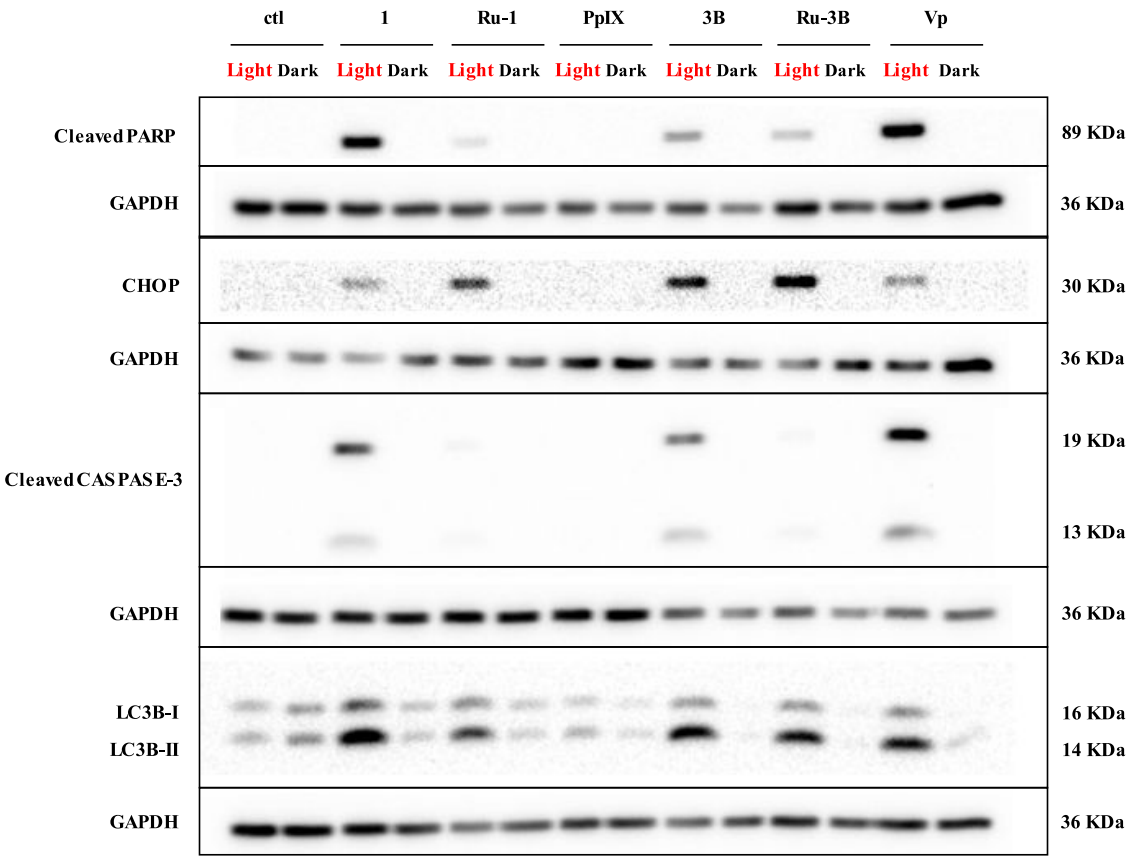

Figure 11. Effects of photoactivation of **1**, **Ru-1**, **3B**, and **Ru-3B** on protein expression on different cell death markers in AGS gastric cancer cells. AGS cells were treated with **1**, **Ru-1**, **3B**, **Ru-3B**, **PpIX**, or **VP** at IC_{50} concentrations for 4 h and then either irradiated with white light or kept in the dark for 15 min and then further cultivated for 24 h in the dark. Protein extraction was performed, and expression of the different markers was determined by Western blot. GAPDH was used as a loading control. Representative Western blot of three independent experiments. ctl = control, untreated cells.

superoxide radical.[81,82] Glutathione peroxidase (GPX4) can suppress lipid peroxidation and protect cells from ferroptosis.[83] To investigate the impact of the different compounds on GPX4 expression, AGS cells were treated as described above, and then GPX4 expression was analyzed by Western blot (Figure 12a). This showed that upon activation by light, **PpIX** and **Ru-3B** lead to a decrease in GPX4 expression (Figure 12a,b), which suggests that these two compounds might induce ferroptosis.

https://doi.org/10.1021/acs.inorgchem.5c00896
Inorg. Chem. 2025, 64, 9684−9702

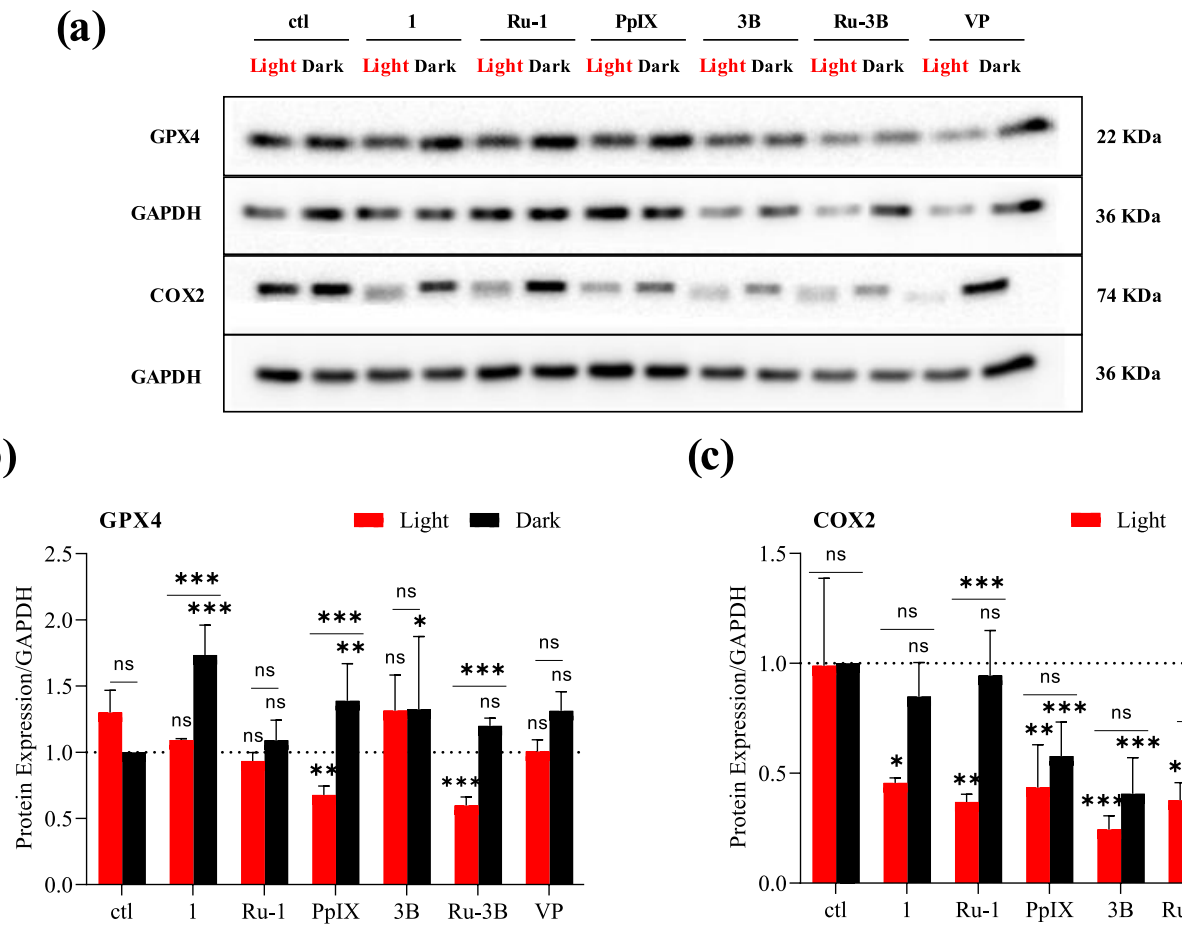

Figure 12. Effects of photoactivation of **1**, **Ru-1**, **3B** and **Ru-3B** on protein expression of ferroptosis and inflammation markers in AGS gastric cancer cells. AGS cells were treated with **1**, **Ru-1**, **3B**, **Ru-3B**, **PpIX**, or **VP** at IC_{50} concentrations for 4 h and then either irradiated with white light or kept in the dark for 15 min and then further cultivated for 24 h in the dark. (a) Expression of the different markers was determined by Western blot. GAPDH was used as a loading control. Representative Western blot of three independent experiments. ctl = control, untreated cells. Graphs represent the quantification of three independent experiments of GPX4 (b) and COX2 (c) expression, compared to not-treated AGS cells (ctl) and normalized to GAPDH expression. Bars above the colons indicate the comparison of dark *versus* light for each compound. The dark and light results of each compound were compared to those of the respective untreated control condition (ctl). Statistical analysis: 2-way Anova *<0.05, **<0.01, ***<0.001, ns = not-significant.

COX2 is known for its central role in inflammation and prostaglandins (PGs) production. In normal cells, COX2 expression is almost absent, whereas in cancer cells, it is frequently overexpressed.[84] Importantly, it has been shown that in cancers, COX2 is not only a mediator of inflammation but could also be a mediator of oxidative stress and inhibition of apoptosis, as well as cancer cell proliferation.[85] The expression of COX2 was analyzed by Western blot (Figure 12a), showing that upon light irradiation, compounds **1** and **Ru-1** significantly reduce COX2 expression compared to untreated conditions. In contrast, **PpIX**, **3B**, **Ru-3B**, and **VP** already lead to a reduction in COX2 expression in the dark (Figure 12a,c). These results suggest that the effect of **PpIX**, **3B**, **Ru-3B**, and **VP** on cell survival upon light activation may not be due to their repressive influence on COX2 expression.

CONCLUSIONS

A series of tetrapyrrole-ruthenium(II) compounds derived from protoporphyrin IX and the commercial drug verteporfin were designed as potential photosensitizers for PDT. The introduction of the ruthenium atom in the central cavity of the macrocycle did not affect the low toxicity in the dark on human gastric cancer cells compared to the free ligands while displaying remarkable cytotoxicity upon irradiation with light. Additionally, our results show that the complexes could cause cell death under low oxygen concentrations by generating singlet oxygen or superoxide anion radicals. Notably, the ruthenium atom coordinated to the chlorin ligands allowed combined mechanisms since EPR studies showed that both singlet oxygen and superoxide radicals could be produced by complexes **Ru-3A** and **Ru-3B** after irradiation. The ruthenium complex **Ru-1** also produced large amounts of singlet oxygen at very low oxygen concentrations. Such results are significant since these new photosensitizers could be used for PDT in hypoxic environments, as often found in tumors. In addition, the study demonstrates that upon light activation, the ruthenium derivatives not only induce cell death *via* a caspase 3 mediated apoptotic pathway, but also partly *via* CHOP, which is an endoplasmic reticulum (ER) stress-inducible transcription factor involved in the development of apoptosis and growth arrest. These data confirm that the new ruthenium compounds can be tuned to trigger various cell death pathways and highlight the potential of our complexes as promising

https://doi.org/10.1021/acs.inorgchem.5c00896
Inorg. Chem. 2025, 64, 9684−9702

multitarget therapeutic alternatives that could reduce tumor resistance mechanisms.

EXPERIMENTAL SECTION

Chemistry. *Reagents and Measurements.* The compounds were synthesized using a double vacuum/inert gas line under a nitrogen or argon atmosphere. All solvents were dried using established procedures and distilled under nitrogen prior to use. All reagents were purchased from Sigma-Aldrich and were used without prior purification. $RuCl_3$ was purchased from Pressure Chemical Company. Ruthenium precursor $[Ru_3(CO)_{12}]$ was prepared according to previously reported procedures.[86]

The reactions were monitored by thin layer chromatography (TLC) using silica gel 60 F_{254} alumina plates (Merck). Infrared spectra were recorded on an α ATR spectrometer from Bruker Optics. Mass spectra (FAB^+) were obtained using a Jeol JMS-SX102A instrument with *m*-nitrobenzyl alcohol as the matrix. Electrospray ionization mass spectrometry (ESI-MS) was performed using a Bruker Esquire spectrometer. The NMR spectra were recorded at room temperature using deuterated chloroform, acetone, or acetonitrile as solvent on a Bruker Advance spectrometer at 300 MHz for proton and 75 MHz for carbon and on a Bruker Advance spectrometer at 500 MHz for proton and 125 MHz for carbon. Chemical shifts (δ) are in ppm downfield of TMS using the residual solvent as an internal standard. Coupling constants (J) are expressed in Hz. Multiplicity: s = singlet, d = doublet, t = triplet, sept = septuplet, m = multiplet. The UV−vis absorption spectra were recorded on a Shimadzu 2600 spectrophotometer in a quartz cuvette at 37 °C with 1×10^{-5} M solutions of each compound in DMSO (prepared from a 10 mM stock solution). The fluorescence spectra were obtained in an Agilent Varian Cary 100 spectrophotometer in quartz cuvettes at room temperature. Electron paramagnetic resonance (EPR) determinations were carried out in an EPR spectrometer (Jeol JES-TE300), operated in the X-Band mode at a modulation frequency of 100 kHz with a cylindrical cavity (TE_{011}). Each sample was placed in a quartz flat cell (Wilmad Glass Company) and irradiated *in situ*. The photogeneration of $^1O_2$ was carried out with a 500 Hg Arc lamp (Oriel OPS-A500), and the samples were irradiated continuously at 160 W. Data acquisition and manipulation were done using the ES-IPRIT/TE program. The HPLC chromatograms were recorded on an Agilent model 1200 Series Binary SL system with a UV−vis detector (λ = 400 nm) and an Eclipse Plus C_{18} (3.5 μm × 2.1 mm) column. The flow rate was 0.2 mL/min, with the initial mobile phase acetonitrile−water (60:40) for the first 10 min. Then acetonitrile−water (90:10) for 20 min and finally acetonitrile for 20 min.

Synthesis of the Ligands. *Synthesis of Porphyrin Derivatives. Porphyrin* ***1****.* The esterification reaction was carried out by adapting a reported procedure.[38] A solution of 95.0 mL of dry methanol and 5.0 mL of H_2SO_4 at 5% (v/v) was cooled to −20 °C in a cold bath, and 1.0 g (1.648 mmol) of the disodium salt of the protoporphyrin IX (**Na_2-PpIX**) was added. The reaction mixture was stirred overnight at −18 °C in the dark. The solution was neutralized with a 10% aqueous solution of $NaHCO_3$, and the organic phase was extracted with 200 mL of $CHCl_3$ and dried over Na_2SO_4. The solvent was evaporated to dryness under vacuum, and the crude solid was purified by column chromatography (silica gel, (1/10) ethyl acetate/dichloromethane) to give 954 mg of a purple solid in 98% yield. The purity observed by HPLC is >99%.

MS (FAB^+) *m*/*z* (%) 591 (30) $[C_{36}H_{38}N_4O_4 + H]^+$. IR (ATR, cm^{-1}): ν−NH 3039, ν_{as}−CH_3 2913, ν_s−CH_3 2852, ν−C═O (ester) 1731. UV−vis (DMSO, λ_{max} nm) (log ε): λ_1 (Soret) 406 (4.48), λ_2 (Q_{IV}) 506 (4.43), λ_3 (Q_{III}) 540 (3.33), λ_4 (Q_{II}) 576 (3.12), λ_5 (Q_I) 630 (2.97). ^{1}H NMR ($CDCl_3$, 300 MHz): −3.84 (s, 2H, NH); 3.27 (t, 4H, ^3J = 7.75, H-22 and H-25); 3.59, 3.60, 3.67, and 3.68 (4s, 18 H, H-17, H-18, H-19, H-20, O−CH_3 and O−CH_3); 4.38 (t, 4H, ^3J = 7.71, H-21 and H-24); 6.18 (dd, 2H, J_{AB} = 1.06, J_{AX} = 11.57, H_A); 6.36 (dd, 2H, J_{BA} = 1.05 Hz, J_{BX} = 17.74 Hz, H_B); 8.25 (m, 2H, H_X); 9.97, 10, 10.11, and 10.13 (4s, 4H, H-α, H-β, H-γ and H-δ). ^{13}C NMR ($CDCl_3$, 75 MHz): 11.81, 12.84, 21.96, 37.06, 51.89, 96.19, 97.18, 97.50, 98.10, 120.90, 130.42, 173.73. The atoms were numbered according to Scheme 1.

Porphyrin ***2****.* The esterification reaction was carried out by adapting a reported procedure.[38]

A solution of 2.0 mL of benzyl alcohol and 0.5 mL of 1.0 N HCl was cooled to −20 °C in a cold bath, and 70 mg (0.115 mmol) of the disodium salt of the protoporphyrin IX (**Na_2-PpIX**) was added. The reaction mixture was stirred overnight at −18 °C in the dark. The solution was neutralized with a 10% aqueous solution of $NaHCO_3$, and the organic phase was extracted with 100 mL of $CHCl_3$ and dried over Na_2SO_4. The solvent was evaporated to dryness under vacuum, and the crude solid was purified by column chromatography (silica gel, (6/4) ethyl acetate/dichloromethane) to give 76 mg of a purple solid in 89% yield. The purity observed by HPLC is >99%.

MS (FAB^+) *m*/*z* (%) 743 (15) $[C_{48}H_{46}N_4O_4 + H]^+$. IR (ATR, cm^{-1}): ν−NH 3306, ν_{as}−CH3 2909, ν_s−CH3 2854, ν−C═O (ester) 1735. UV−vis (DMSO, λ_{max} nm) (log ε): λ_1 (Soret) 408 (4.76), λ_2 (Q_{IV}) 506 (3.87), λ_3 (Q_{III}) 540 (3.77), λ_4 (Q_{II}) 576 (3.56), λ_5 (Q_I) 630 (3.41). ^{1}H NMR ($CDCl_3$, 300 MHz): −3.87 (s, 2H, NH); 3.30 (t, 4H, ^3J = 7.55, H-22 and H-25); 3.55 and 3.67 (2s, 12 H, H-17, H-18, H-19 and H-20); 4.38 (t, 4H, ^3J = 7.51, H-21 and H-24); 5.04 (s, 4H, Ph−CH_2); 6.18 (dd, 2H, J_{AB} = 1.01, J_{AX} = 11.56, H_A); 6.37 (dd, 2H, J_{BA} = 1.68, J_{BX} = 17.80, H_B); 7.03 (m, 10H, Ph-H); 8.25 (dd, 2H, J_{XA} = 11.44, J_{XB} = 17.17, H_X); 9.96, 9.97, 10.07, and 10.13 (4s, 4H, H-α, H-β, H-γ and H-δ). ^{13}C NMR ($CDCl_3$, 75 MHz): 11.83, 12.87, 21.94, 37.18, 66.51, 96.37, 97.25, 97.56, 98.11, 120.93, 128.07, 128.14, 128.41, 130.44, 135.84, 173.14. The atoms were numbered according to Scheme 1.

Synthesis of Chlorin Derivatives. The Diels−Alder reaction was carried out by modifying a reported procedure.[39,40] Dimethyl acetylenedicarboxylate (1.0 mL, 0.008 mol) was added to a solution of 100 mg of the porphyrin **1** or **2** in 5 mL of chloroform. The reaction mixture was heated to reflux temperature for 72 h with constant stirring. The reaction was concentrated under vacuum, and the two isomers were separated by silica gel chromatography using dichloromethane/hexane/ethyl acetate as eluent (8:1.2:0.8).

Chlorin ***3A****.* Dark blue solid, 19 mg, 21% yield. The purity observed by HPLC is >99%. MS (ESI) *m*/*z* 733 $[C_{42}H_{44}N_4O_8+H]^+$. IR (ATR, cm^{-1}): ν−NH 3334, ν_{as}−CH_3 2948, ν_s−CH_3 2856, ν−C═O (ester) 1721. UV−vis (DMSO, λ_{max} nm) (log ε): λ_1 (Soret) 406 (4.92), λ_2 (Q_{IV}) 502 (4.05), λ_3 (Q_{III}) 536 (3.94), λ_4 (Q_{II}) 608 (3.60), λ_5 (Q_I) 666 (4.51). ^{1}H NMR ($CDCl_3$, 300 MHz): −2.63 (s, 2H, NH); 2.11 (s, 3H, H-18); 3.26 (t, 2H, J = 7.79, H-25); 3.24 (t, 2H, J = 7.85, H-22); 3.37 (s, 3H, H-19); 3.52 (a, 3H, H-20); 3.54 (s, 3H, H-17); 3.60 (dd, 1H, J = 1.90, H-28); 3.68 (s, 3H, O−CH_3); 3.69 (s, 3H, O−CH_3); 3.93 (s, 3H, H-31); 4.02 (dd, 1H, J = 6.67, H-28); 4.07 (s, 3H, H-32); 4.16 (t, 2H, J = 7.61, H-24); 4.36 (t, 2H, J = 7.23, H-21); 6.14 (dd, 1H, J_{AB} = 1.46, J_{AX} = 11.51, H_A); 6.32 (dd, 1H, J_{BA} = 1.43, J_{BX} = 17.84, H_B); 7.39 (dd, 1H, J = 1.97, J = 6.61, H-27); 8.11 (dd, 1H, J_{XA} = 11.49, J_{XB} = 17.79, H_X); 9.13 (s, 1H, H-δ); 9.34 (s, 1H, H-α); 9.74 (s, 1H, H-γ); 9.76 (s, 1H, H-β). ^{13}C NMR ($CDCl_3$, 75 MHz): 11.54, 11.73, 12.40, 21.71, 21.95, 28.33, 29.95, 36.78, 37.17, 51.82, 51.93, 52.57, 52.73, 54.93, 90.54, 92.44; 99.03, 99.49, 118.39, 121.63, 128.77, 129.76, 129.86, 130.58, 133.19, 133.22, 134.16, 136.26, 137.28, 138.08, 138.26, 140.05, 149.25, 149.35, 150.56, 151.93, 152.22, 162.39, 166.21, 170.28, 173.52, 173.90. The atoms were numbered according to Scheme 1.

Chlorin ***3B****.* Brown solid, 61 mg, 68% yield. The purity observed by HPLC is >99%. MS (ESI) *m*/*z* 733 $[C_{42}H_{44}N_4O_8+H]^+$. IR (ATR, cm^{-1}): ν−NH 3339, ν_{as}−CH_3 2957, ν_s−CH_3 2854, ν−C═O (ester) 1717. UV−vis (DMSO, λ_{max} nm) (log ε): λ_1 (Soret) 404 (5.03), λ_2 (Q_{IV}) 500 (4.07), λ_3 (Q_{III}) 534 (3.93), λ_4 (Q_{II}) 608 (3.62), λ_5 (Q_I) 666 (4.55). ^{1}H NMR ($CDCl_3$, 300 MHz): −2.48 (s, 2H, NH); 2.11 (s, 3H, H-18); 3.20 (2 t, superimposed, 4H; H-22 and H-25); 3.42 (s, 3H, H-20); 3.49 (s, 3H, H-17); 3.62 (dd, 1H, J = 1.88, J = 21.03, H-28); 3.66 (s, 6H, O−CH_3); 3.67 (s, 3H, H-19); 3.91 (s, 3H, H-31); 3.98 (dd, 1H, J = 6.68, J = 21.07, H-28); 4.01 (s, 3H, H-32); 4.17 (t, 2H, ^3J = 7.54, H-21); 4.31 (t, 2H, ^3J = 7.57, H-24); 6.17 (dd, 1H, J_{AX} = 11.62, H_A); 6.34 (dd, 1H, J_{BX} = 17.78, H_B); 7.39 (dd; 1H, ^3J = 6.37, H-27); 8.18 (dd, 1H; J_{XA} = 11.55, J_{XB} = 17.79, H_X); 9.22 (s, 1H; H-

https://doi.org/10.1021/acs.inorgchem.5c00896
Inorg. Chem. 2025, 64, 9684−9702

α); 9.31 (s, 1H, H-β); 9.66 (s, 1H, H-γ); 9.80 (s, 1H, H-δ). ^{13}C NMR ($CDCl_3$, 75 MHz): 11.43, 11.80, 12.78, 21.67, 21.98, 28.33, 29.96, 36.74, 37.17, 51.83, 51.92, 52.71, 52.75, 54.82, 90.11, 92.77, 98.25, 100.42, 118.77, 120.87, 128.52, 129.72, 130.77, 131.10, 133.28, 133.32, 134.14, 136.51, 136.90, 138.25, 138.52, 139.75, 149.31, 149.39, 151.03, 151.27, 153.03, 162.31, 166.19, 170.21, 173.50, 173.92. The atoms were numbered according to Scheme 1.

Chlorin ***4A***. Dark blue solid, 7 mg, 19% yield. The purity observed by HPLC is >99%. MS (ESI) *m*/*z* 885 $[C_{54}H_{52}N_4O_8+H]^+$. IR (ATR, cm^{-1}): ν−NH 3341, ν_{as}−CH_3 2953, ν_s−CH_3 2850, ν−C═O (ester) 1718. UV−vis (DMSO, λ_{max} nm) (log ε): λ_1 (Soret) 406 (5.01), λ_2 (Q_{IV}) 502 (3.97), λ_3 (Q_{III}) 536 (3.87), λ_4 (Q_{II}) 608 (3.60), λ_5 (Q_I) 666 (4.42). ^{1}H NMR ($CDCl_3$, 300 MHz): −2.58 (s, 2H, NH); 2.11 (s, 3H, H-18); 3.24 (2 t, superimposed, 4H, H-22 and H-25); 3.37 (s, 3H, H-20); 3.48 (s, 3H, H-19); 3.59 (s, 3H, H-17); 3.67 (dd, 1H, *J* = 1.76, H-28); 3.91 (s, 3H, H-31); 4.00 (dd, 1H, *J* = 6.76, H-28); 4.01 (s, 3H, H-32); 4.20 (t, 2H, ^3J = 7.52, H-21); 4.35 (t, 2H, ^3J = 7.61, H-24); 5.04 (s, 4H, Ph−CH_2); 6.17 (dd, 1H, J_{AB} = 1.15, J_{AX} = 11.60, H_A); 6.37 (dd, 1H, J_{BA} = 1.46, J_{BX} = 17.87, H_B); 7.06 (m, 10H; Ph-H); 7.41 (dd; 1H, *J* = 1.75, *J* = 6.42, H-27); 8.18 (dd, 1H; J_{XA} = 11.52, J_{XB} = 17.73, H_X); 9.09 (s, 1H; H- δ); 9.39 (s, 1H, H-α); 9.77 (s, 1H, H-γ); 9.82 (s, 1H, H-β). ^{13}C NMR ($CDCl_3$, 75 MHz): 11.45, 11.81, 12.79, 21.65, 21.97; 28.32, 29.97, 36.88, 37.30, 52.72, 52.76, 54.82, 66.43; 66.55, 90.15, 92.74, 98.42, 100.47, 118.73, 120.86, 124.95, 128.05, 128.53, 129.75, 130.74, 131.18, 133.25, 133.31, 134.19, 136.23, 136.88, 138.25, 138.62, 139.74, 149.34, 149.41, 151.05, 151.36, 153.00, 162.28, 166.21, 170.23, 172.94, 173.35. The atoms were numbered according to Scheme 1.

Chlorin ***4B***. Brown solid, 17 mg, 44% yield. The purity observed by HPLC is >99%. MS (ESI) *m*/*z* 885 $[C_{54}H_{52}N_4O_8 + H]^+$. IR (ATR, cm^{-1}): ν−NH 3341, ν_{as}−CH_3 2923, ν_s−CH_3 2852, ν−C═O (ester) 1719. UV−vis (DMSO, λ_{max} nm) (log ε): λ_1 (Soret) 406 (4.99), λ_2 (Q_{IV}) 502 (4.10), λ_3 (Q_{III}) 534 (3.94), λ_4 (Q_{II}) 608 (3.60), λ_5 (Q_I) 666 (4.59). ^{1}H NMR ($CDCl_3$, 300 MHz): −2.55 (s, 2H, NH); 2.04 (s, 3H, H-18); 3.15 (2 t, superimposed, 4H, H-22 and H-25); 3.31 (s, 3H, H-20); 3.37 (s, 3H, H-19); 3.55 (dd, 1H, *J* = 1.97, H-28); 3.59 (s, 3H, H-17); 3.82 (s, 3H, H-31); 3.90 (dd, 1H, *J* = 6.66, *J* = 22.15, H-28); 3.94 (s, 3H, H-32); 4.11 (t, 2H, ^3J = 7.52, H-21); 4.24 (t, 2H, ^3J = 7.61, H-24); 4.94 (s, 2H, Ph−CH_2); 4.97 (s, 2H, Ph−CH_2); 6.10 (dd, 1H, J_{AB} = 1.43, J_{AX} = 11.54, H_A); 6.26 (dd, 1H, J_{BA} = 1.43, J_{BX} = 17.88, H_B); 6.95−7.07 (m, 10H, Ph-H); 7.31 (dd; 1H, *J* = 2.01, *J* = 6.68, H-27); 8.11 (dd, 1H; J_{XA} = 11.57, J_{XB} = 17.84, H_X); 9.15 (s, 1H, H-α); 9.21 (s, 1H, H-β); 9.60 (s, 1H, H-γ); 9.71 (s, 1H, H-δ). ^{13}C NMR ($CDCl_3$, 75 MHz): 11.45, 11.81, 12.79, 21.65, 21.97, 28.32, 29.97, 36.88, 37.30, 52.72, 52.76, 54.82, 66.43, 66.55, 90.15, 92.74, 98.42, 100.47, 118.73, 120.86, 124.95, 128.05, 128.53, 129.75, 130.74, 131.18, 133.25, 133.31, 134.19, 136.23, 136.88, 138.25, 138.62, 139.74, 149.34, 149.41, 151.05, 151.36, 153.00, 162.28, 166.21, 170.23, 172.94, 173.35. The atoms were numbered according to Scheme 1.

Synthesis of the Complexes. General Procedure. The ruthenium complexes were prepared by adapting a reported procedure.[41] A solution of 1.0 mmol of the corresponding ligand (**1**, **2**, **3A**, and **3B**) and 1.1 mmol of $[Ru_3(CO)_{12}]$ in 10 mL of benzene was stirred at reflux temperature for 24 h in the dark. The solvent was evaporated to dryness under vacuum, and the crude solid was purified through column chromatography on neutral alumina using a 1:2 hexane/acetone mixture as eluent.

Ru-1: A pink solid was obtained from 30.0 mg (0.051 mmol) of **1** and 36.0 mg (0.056 mmol) of $[Ru_3(CO)_{12}]$ in 78% yield (28 mg). The purity observed by HPLC is >99%. MS (FAB^+) *m*/*z* 718 $[C_{37}H_{36}N_4O_5Ru + H]^+$. IR (ATR, cm^{-1}): ν_{as}−CH_3 2921, ν_s−CH_3 2858, ν−Ru−C═O 1914, ν−C═O (ester) 1744. UV−vis (DMSO, λmax nm) (log ε): λ_1 (Soret) 404 (4.76), λ_2 (Q_β) 524 (4.08), λ_3 (Q_α) 558 (4.27). ^{1}H NMR (CD_3CN, 500 MHz): 3.30 (t, 4H, H-22 and H-25); 3.57, 3.59, 3.60, 3.61, 3.70, and 3.71 (6s, 18H, H-17, H-18, H-19, H-20, O−CH_3 and O−CH_3); 4.33 (t, 4H, H-21 and H-24); 6.11 (dd, 2H, J_{AB} = 1.52, J_{AX} = 11.51, H_A); 6.40 (dd, 2H, J_{BA} = 1.49, J_{BX} = 17.82, H_B); 8.38 (m, 2H, J_{XA} = 11.47, J_{XB} = 17.85, H_X); 9.94, 10.06, 10.10, 10.17 (4s, 4H, H-α, H-β, H-γ and H-δ). ^{13}C NMR (CD_3CN, 125 MHz): 11.72, 12.94, 14.32, 22.38, 23.29, 30.83, 32.26, 37.56, 52.06, 99.34, 100.01, 100.21, 100.67, 119.87, 174.46, 207.46 (Ru-CO). The atoms were numbered according to Scheme 2.

Ru-2: A pink solid was obtained from 30.0 mg (0.041 mmol) of **2** and 28.0 mg (0.044 mmol) of $[Ru_3(CO)_{12}]$ in 61% yield (21 mg). The purity observed by HPLC is >99%. MS (ESI) *m*/*z* (%) 872 $[C_{37}H_{36}N_4O_5Ru + 2H]^+$. IR (ATR, cm^{-1}): ν_{as}−CH_3 2922, ν_s−CH_3 2859, ν−Ru−C═O 1915, ν−C═O (ester) 1729. UV−vis (DMSO, λmax nm) (log ε): λ_1 (Soret) 402 (4.76), λ_2 (Q_β) 524 (4.08), λ_3 (Q_α) 558 (4.11). ^{1}H NMR (CD_3CN, 500 MHz): 3.36 (t, 4H, H-22 and H-25); 3.52, 3.55, 3.70, and 3.71 (4s, 12H, H-17, H-18, H-19 and H-20); 4.34 (t, 4H, H-21 and H-24); 5.05 (s, 4H, Ph−CH_2); 6.11 (dd, 2H, J_{AB} = 1.72, J_{AX} = 11.54, H_A); 6.40 (dd, 2H, J_{BA} = 1.78, J_{BX} = 17.89, H_B); 7.13 (m, 10H, Ph-H); 8.40 (dd, 2H, J_{XA} = 11.75, J_{XB} = 17.58, H_X); 9.98, 10.04, 10.08, and 10.17 (4s, 4H, H-α, H-β, H-γ and H-δ). ^{13}C NMR (CD_3CN, 125 MHz): 11.58, 11.79, 18.07, 20.26, 22.52, 29.70, 37.87, 37.93, 66.78, 99.18, 99.36, 99.39, 99.52, 128.58, 128.70, 128.79, 129.29, 129.32, 131.32, 131.42, 136.81, 136.91, 137.47, 138.04, 138.06, 140.02, 140.05, 142.01, 142.34, 142.57, 143.02, 143.05, 143.31, 143.36, 143.91, 144.02, 174.01, 211.04 (Ru-CO). The atoms were numbered according to Scheme 2.

Ru-3A: A green solid was obtained from 30.0 mg (0.041 mmol) of **3A** and 29.0 mg (0.045 mmol) of $[Ru_3(CO)_{12}]$ in 13% yield (4 mg). The purity observed by HPLC is >98%. MS (ESI) *m*/*z* (%) 862 $[C_{43}H_{42}N_4O_9Ru + 2H]^+$. IR (ATR, cm^{-1}): ν_{as}−CH_3 2992, ν_s−CH_3 2854, ν−Ru−C═O 1927, ν−C═O (ester) 1722. UV−vis (DMSO, λmax nm) (log ε): λ_1 (Soret) 406 (4.83), λ_2 (Q_β) 536 (3.81), λ_3 (Q_α) 568 (3.94), λ_4 (Q_γ) 606 (4.24). ^{1}H RMN (acetone-d_6, 300 MHz): 2.83 (s, 3H, H-18); 3.14 (t, 2H, H-22); 3.26 (t, 2H, H-25); 3.31 (s, 3H, H-19); 3.55 (s, 3H, H-20); 3.56 (s, 3H, H-17) 3.57 (dd, 1H, *J* = 2.39, H-28); 3.61 (s, 3H, O−CH_3); 3.62 (s, 3H, O−CH_3); 3.66 (dd, 1H, *J* = 7.59, H-28); 3.90 (s, 3H, H-31); 4.08 (s, 3H, H-32); 4.11 (t, 2H, H-24); 4.37 (t, 2H, H-21); 6.14 (dd, 1H, J_{AB} = 1.58, J_{AX} = 11.62, H_A); 6.37 (dd, 1H, J_{BA} = 1.63, J_{BX} = 17.91, H_B), 7.65 (dd, 1H, *J* = 2.30, H-27), 8.23 (dd, 1H, J_{XA} = 11.67, J_{XB} = 17.88, H_X), 9.20 (s, 1H, H- δ), 9.55 (s, 1H, H-α), 9.77 (s, 1H, H-γ), 9.91 (s, 1H, H-β). ^{13}C NMR (acetone-d_6, 75 MHz): 11.43, 11.50, 12.35, 21.97, 22.17, 37.04, 37.47, 51.69, 51.80, 52.00, 52.79, 91.49, 93.15, 99.95, 100.39, 120.57, 121.95, 127.14, 130.47, 137.91, 141.39, 143.33, 149.10, 149.49, 151.67, 152.00, 152.75, 163.53, 166.63, 173.68, 173.87. The atoms were numbered according to Scheme 2.

Ru-3B: A green solid was obtained from 30.0 mg (0.041 mmol) of **3B** and 29.0 mg (0.045 mmol) of $[Ru_3(CO)_{12}]$ in 16% yield (6 mg). The purity observed by HPLC is >98%. MS (ESI) *m*/*z* (%) 862 $[C_{43}H_{42}N_4O_9Ru + 2H]^+$. IR (ATR, cm^{-1}): ν_{as}−CH_3 2923, ν_s−CH_3 2857, ν−Ru−C═O 1923, ν−C═O (ester) 1721. UV−vis (DMSO, λmax nm) (log ε): λ_1 (Soret) 406 (4.63), λ_2 (Q_β) 534 (3.66), λ_3 (Q_α) 568 (3.83), λ_4 (Q_γ) 606 (4.02). ^{1}H NMR (acetone-d_6, 300 MHz): 2.79 (s, 3H, H-18); 3.17 (t, 2H, H-22); 3.25 (t, 2H, H-25); 3.42 (s, 3H, H-20); 3.54 (s, 3H, H-17); 3.60 (s, 3H, O−CH_3); 3.61 (s, 3H, O−CH_3); 3.68 (s, 3H, H-19); 3.76 (d, 1H, H-28) 3.88 (s, 3H, H-31); 4.00 (d, 1H, H-28); 4.03 (s, 3H, H-32); 4.16 (t, 2H); 4.34 (t, 2H); 6.21 (dd, 1H, J_{AB} = 1.447, J_{AX} = 11.586, H_A); 6.39 (dd, 1H, J_{BA} = 1.466, J_{BX} = 17.892, H_B); 7.68 (dd; 1H, ^3J = 6.775, H-27); 8.21 (dd, 1H; J_{XA} = 11.603, J_{XB} = 17.852, H_X); 9.31 (s, 1H, H-α); 9.55 (s, 1H, H-β); 9.87 (s, 1H, H-γ); 9.95 (s, 1H, H-δ). ^{13}C NMR (acetone-d_6, 75 MHz): 11.15, 11.49, 12.52, 21.84, 22.14, 36.92, 37.42, 51.69, 51.78, 52.79, 52.92, 55.07, 90.98, 93.37, 99.35, 101.34, 120.89, 121.36, 130.02, 130.36, 137.01, 137.92, 139.05, 139.39, 149.55, 151.84, 152.45, 154.25, 163.23, 166.61, 170.32, 173.63, 173.88. The atoms were numbered according to Scheme 2.

Crystallography. Single crystals suitable for X-ray diffraction were obtained for **3B** and **Ru-1** by slow evaporation of dichloromethane/hexane solution. Data were collected at room temperature (298 K) on a Bruker Apex-II CCD diffractometer using monochromatic graphite Mo Kα (0.71073Å) radiation. Cell determination and final cell parameters were obtained on all reflections using the Bruker SAINT software included in the APEX2 software.[87,88] The integration and scaling of the data were carried out using the Bruker SAINT software.[87,88] For compound **3B**, weak high-angle diffractions,

https://doi.org/10.1021/acs.inorgchem.5c00896
Inorg. Chem. 2025, 64, 9684−9702

combined with the multiple contents and some degree of disorder, caused a large number of refined parameters with poor data/parameters ratio, which led to the observed low C−C precision. However, the identity of the structure was clearly established without issue. The CIF files have been deposited in the Cambridge Structural Data Base under CCDC 2400652 for **3B** and 2400653 for **Ru-1**. Copies of the data can be obtained, free of charge, at www.ccdc.cam.ac.uk.

Stability Studies. Stability studies were performed using a Shimadzu 2600 UV−vis spectrophotometer at 37 °C from 1×10^{-5} M solutions of each compound in pure DMSO or in PBS (Dulbecco's Phosphate Buffered Saline, Dominique Dutscher SAS without magnesium and calcium) with 0.1% DMSO. Spectra were recorded every hour for 24 h in DMSO and every hour for 8 h in PBS/DMSO (0.1%).

Photostability Studies. The photodegradation of the new compounds was evaluated as described in the literature.[46] Solutions of each compound at a concentration of 1×10^{-5} M were prepared in pure DMSO or in PBS/DMSO (0.1%). Each solution was irradiated at 37 °C with white light (light temperature: 8500 K and light intensity: 50%, SmallRing brand) at different times until completing 15 min (irradiation time: 0, 3, 6, 9, 12, and 15 min). The absorption spectrum was recorded after each irradiation.

EPR Studies. The detection of singlet oxygen is based on the specific reaction between $^1O_2$ and 2,2,6,6-tetramethylpiperidine (TEMP), which produces a stable (2,2,6,6-tetramethylpiperidin-1-yl)oxyl (TEMPO) radical adduct. Detection of $^1O_2$ was carried out according to the following procedure. Solutions of 1×10^{-3} M of the compounds and 0.06 M TEMP in ethanol/DMSO (1%, final volume 400 μL) equilibrated with air at room temperature were irradiated with visible light in a flat cell for up to 15 min, generating the characteristic triplet signal corresponding to TEMPO. EPR spectra were obtained with the following parameters: center field, 334.5 ± 4 mT; power, 1.0 mW; microwave frequency, 9.43 GHz; modulation width, 0.5 mT; time constant, 0.1 s; amplitude, 10. The oxygen concentration was measured using an Iuzmar dissolved oxygen meter. For the detection of superoxide radical ($O_2^{\bullet-}$), 5,5-dimethyl-1-pyrroline-*N*-oxide (DMPO, from Dojindo Japan) was used. Detection of $O_2^{\bullet-}$ was carried out according to the following procedure. A mixture of 1×10^{-3} M solution of the compounds and a 0.07 M solution of DMPO in methanol/DMSO (1%, final volume 400 μL) at room temperature were irradiated with visible light in a flat cell for up to 15 min, generating the signal of the DMPO-$O_2^{\bullet-}$ adduct. EPR spectra were obtained with the following parameters: center field, 335 ± 4 mT; power, 8.0 mW; microwave frequency, 9.43 GHz; modulation width, 0.63 mT; time constant, 0.1 s; amplitude, 100.

Fluorescence Quantum Yield Measurements. The fluorescence quantum yields were determined using verteporfin in DMSO as a reference ($\Phi_f = 0.0085$).[46,89] The free ligands were excited at 503 nm, and the ruthenium complexes at 573 nm. The quantum yield was calculated following eq 1.[90,91]

$$\Phi_f = \Phi_{ST}\left(\frac{\text{grad}_X}{\text{grad}_{ST}}\right)\left(\frac{\eta_X^2}{\eta_{ST}^2}\right) \quad (1)$$

Where ST and X are standard and analyte, respectively, Φ_f is the fluorescence quantum yield, Grad is the gradient from the area of integration fluorescence intensity *vs* absorbance, and η_X and η_{ST} are the refractive index of the solvent used to measure the fluorescence spectrum of the analyte and the standard, respectively.

Oxygen Singlet Quantum Yield Measurements. Quantum yields of singlet oxygen ($^1O_2$) production were determined in DMSO equilibrated with oxygen and white light, using verteporfin as a reference and 1,3-diphenylisobenzofuran (DPBF) as a chemical trap which in the presence of singlet oxygen is oxidized to 1,2-dibenzoylbenzene.[92] The absorption band of DPBF was monitored at 214 nm.[93] The $^1O_2$ production quantum yields of the compounds were determined following eq 2.[94,95]

$$\Phi_{\Delta PS} = \Phi_{\Delta ref}\frac{k_{PS}}{k_{ref}} \quad (2)$$

Where PS is the photosensitizer, $\Phi_{\Delta ref}$ is singlet oxygen production quantum yield of verteporfin ($\Phi_\Delta = 0.77$ in DMSO[46]) and k_{ref} and k_{PS} are the decay constant of DPBF in the presence of the standard (VP) or each PS and are obtained from the slope obtained from the absorbance of DPBF at different irradiation times.

Lipophilicity Studies. The partition coefficient ($\log P_{o/PBS}$) of each compound was determined experimentally by the "*shake-flask*" method at room temperature following reported methods.[57,96] A mixture of 1-octanol and PBS in equal amounts was shaken for 24 h, after which the phases were allowed to separate for 24 h. Then, a 1×10^{-5} M solution of each compound is prepared in 1-octanol/PBS (1:1), and the mixture is left to stir for 24 h. After 24 h of stirring, the mixture is left for 24 h to separate the two phases. Finally, the concentration of each compound in the two phases is determined by UV−vis spectroscopy. log*P* was determined by the following eq 3.[97]

$$\log P = \log\left(\frac{A_{ap}}{A_{bp} - A_{ap}}\right) \quad (3)$$

Where A_{ap} is the absorbance after partition, and A_{bp} is the absorbance before partition.

Biology. *Cell Lines.* The human gastric adenocarcinoma (AGS) cell line was acquired from ATCC (Manassa, VA). AGS cells were cultured in RPMI 1640 medium (Roswell Park Memorial Institute) containing 10% fetal bovine serum (FBS) at 37 °C in a humidified atmosphere of 95% air and 5% CO_2.

MTT Survival Assays. The antiproliferative activity of cancer cells was determined by the 3-(4,5-dimethylthiazol-2-yl)-2,5-diphenyltetrazolium bromide (MTT) assay. Cells were seeded at 10.000 cells per well (200 μL) in Cellstar 96-well plates (Greiner Bio-One) and further incubated for 24 h. Cells were treated with each compound at different concentrations for 8 h in the dark. After this time, the medium was removed, fresh medium was added, and cells were kept in the dark or irradiated with white light for 15 min. Subsequently, the plates were incubated in the dark for an additional 48 h, and the MTT assay was performed as previously described in the literature.[34] Measurements were performed at 550 nm with the Tristar2Multimode Reader (Berthold Technologies).

Western Blotting.[98] AGS cells were treated with the IC_{50} of each compound for 4 h at 37 °C in the dark and then were either kept in the dark or irradiated with white light for 15 min and further cultivated in the dark for an additional 24 h. Cells were then lysed in lysis buffer (50 mM Tris−HCl pH 6.7, NaCl 150 mM, NP40 1%). Total protein concentration was determined using Bradford assay and adjusted to the same quantity (50 μg) for each experiment. A total of 30 μg of proteins were resolved by 6−15% SDS-PAGE (depending on protein molecular weight) and transferred to nitrocellulose blotting membranes according to standard methods. Membranes were blocked with blocking buffer (containing 5% milk powder or 1% BSA) for 1 h at room temperature, then washed three times with TBST or PBST (containing 0.1% Tween-20) and incubated with primary antibodies at 4 °C overnight. The following day, the membranes were washed thrice with PBST or PBST. The membranes were incubated with antirabbit or antimouse antibodies for 1 h at room temperature and visualized by enhanced chemiluminescence using the ClarityTM ECL Western Blotting Substrate Bio-Rad reagent according to the manufacturer's instructions. Signals were acquired with the help of Immobilon Crescendo or Ozyme on Syngene PX*i* equipment using GeneSys software. Protein bands were quantified using ImageJ software.[99] Western blots were performed using the following antibodies: GAPDH (6C5) (1:2000, sc-32233, Santa Cruz Biotechnology); Cleaved PARP (D64E10) (1:1000, 5625S, Cell Signaling Technology); COX2 (D5H5) (1:1000, 12282S, Cell Signaling Technology); CHOP/GADD 153 (B-3) (1:500, sc-7351, Santa Cruz Biotechnology); Cleaved Caspase-3 (D175) (1:1000, 9661L, Cell Signaling Technology); GPX4 (1:1000, ab25066, abcan) and LC3B (D11) (1:1000, 3868S, Cell Signaling Technology). The

https://doi.org/10.1021/acs.inorgchem.5c00896
Inorg. Chem. 2025, 64, 9684−9702

secondary antibodies were: Antirabbit IgG (1:10000, 7074S, Cell Signaling Technology) and Anti-Mouse IgG (1:8000, 7076S, Cell Signaling Technology). Loading was controlled by glyceraldehyde-3-phosphate dehydrogenase (GAPDH) for normalization.

■ ASSOCIATED CONTENT

Supporting Information

The Supporting Information is available free of charge at https://pubs.acs.org/doi/10.1021/acs.inorgchem.5c00896.

Mass spectra; IR spectra; NMR spectra; UV−vis spectra; EPR spectra and cell survival graphs (Figures S1−S102); crystallographic data and quantum yields (Tables S1 and S2) (PDF)

Accession Codes

Deposition Numbers 2400652−2400653 contain the supplementary crystallographic data for this paper. These data can be obtained free of charge *via* the joint Cambridge Crystallographic Data Centre (CCDC) and Fachinformationszentrum Karlsruhe Access Structures service.

■ AUTHOR INFORMATION

Corresponding Authors

Georg Mellitzer − *Inserm UMR_S U1113; IRFAC, 67200 Strasbourg, France;* Present Address: INSERM, UMR_S1260, Regenerative Nanomedicine; Team GP-SMIT; CRBS, 1 Rue Eugène Boeckel, 67085 Strasbourg, France; Email: mellitzer@unistra.fr

Ronan Le Lagadec − *Universidad Nacional Autonoma de México, Instituto de Química UNAM, 04510 Ciudad de México, Mexico;* orcid.org/0000-0002-5679-2081; Email: ronan@unam.mx

Authors

Andrés Restrepo-Acevedo − *Universidad Nacional Autonoma de México, Instituto de Química UNAM, 04510 Ciudad de México, Mexico*

María Isabel Murillo − *Universidad Nacional Autonoma de México, Instituto de Química UNAM, 04510 Ciudad de México, Mexico*

Christophe Orvain − *Inserm UMR_S U1113; IRFAC, 67200 Strasbourg, France;* Present Address: INSERM, UMR_S1260, Regenerative Nanomedicine; Team GP-SMIT; CRBS, 1 Rue Eugène Boeckel, 67085 Strasbourg, France

Chloé Thibaudeau − *Inserm UMR_S U1113; IRFAC, 67200 Strasbourg, France*

Sevda Recberlik − *Inserm UMR_S U1113; IRFAC, 67200 Strasbourg, France;* Present Address: INSERM, UMR_S1260, Regenerative Nanomedicine; Team GP-SMIT; CRBS, 1 Rue Eugène Boeckel, 67085 Strasbourg, France

Lucas Verget − *Universidad Nacional Autonoma de México, Instituto de Química UNAM, 04510 Ciudad de México, Mexico; Faculté de Chimie, Sorbonne Université, 75005 Paris, France*

Virginia Gómez Vidales − *Universidad Nacional Autonoma de México, Instituto de Química UNAM, 04510 Ciudad de México, Mexico*

Christian Gaiddon − *Inserm UMR_S U1113; IRFAC, 67200 Strasbourg, France;* Present Address: UMR7242, Biotechnology et Signalisation Cellulaire, 300 Boulevard S. Brant, 67412 Illkirch Cedex, France; orcid.org/0000-0003-4315-3851

Complete contact information is available at: https://pubs.acs.org/10.1021/acs.inorgchem.5c00896

Author Contributions

The manuscript was written with contributions from all authors. All authors have approved the final version of the manuscript.

Notes

The authors declare no competing financial interest.

■ ACKNOWLEDGMENTS

We wish to thank the financial support from DGAPA-UNAM (PAPIIT projects IN-211522 and IN207725), Consejo Nacional de Ciencia y Tecnología (Project A1-S-15068 and grant 996154 to A. Restrepo-Acevedo), ECOS Nord (Project 279063), and the Long Duration National or International Academic Activities program from the General Coordination of Graduate Studies at UNAM. We thank M. P. Orta Perez, A. Romo, L. del Carmen Márquez, E. García Ríos, L. Rios Ruiz, J. D. Vázquez Cuevas, M. M. Aguilar Araiza, G. E. Cortés Romero, and N. Perrusson for obtaining analytical data and for technical assistance. Rubén A. Toscano is thanked for X-ray diffraction crystallographic studies.

■ REFERENCES

(1) Oluwajembola, A. M.; Cleanclay, W. D.; Onyia, A. F.; Chikere, B. N.; Zakari, S.; Ndifreke, E.; De Campos, O. C. Photosensitizers in photodynamic therapy: An advancement in cancer treatment. *Results Chem.* **2024**, *10*, No. 101715.

(2) Zhang, Y.; Doan, B. T.; Gasser, G. Metal-Based Photosensitizers as Inducers of Regulated Cell Death Mechanisms. *Chem. Rev.* **2023**, *123* (16), 10135−10155.

(3) Alderden, R. A.; Hall, M. D.; Hambley, T. W. The Discovery and Development of Cisplatin. *J. Chem. Educ.* **2006**, *83* (5), No. 728.

(4) Johnstone, T. C.; Suntharalingam, K.; Lippard, S. J. The Next Generation of Platinum Drugs: Targeted Pt(II) Agents, Nanoparticle Delivery, and Pt(IV) Prodrugs. *Chem. Rev.* **2016**, *116* (5), 3436−3486.

(5) Kelland, L. The resurgence of platinum-based cancer chemotherapy. *Nat. Rev. Cancer* **2007**, *7* (8), 573−584.

(6) Florea, A.-M.; Büsselberg, D. Cisplatin as an Anti-Tumor Drug: Cellular Mechanisms of Activity, Drug Resistance and Induced Side Effects. *Cancers* **2011**, *3* (1), 1351−1371.

(7) Klein, A. V.; Hambley, T. W. Platinum Drug Distribution in Cancer Cells and Tumors. *Chem. Rev.* **2009**, *109* (10), 4911−4920.

(8) Aebisher, D.; Serafin, I.; Batóg-Szczęch, K.; Dynarowicz, K.; Chodurek, E.; Kawczyk-Krupka, A.; Bartusik-Aebisher, D. Photodynamic Therapy in the Treatment of Cancer—The Selection of Synthetic Photosensitizers. *Pharmaceuticals* **2024**, *17* (7), No. 932.

(9) Zhang, Y.; Doan, B.-T.; Gasser, G. Metal-Based Photosensitizers as Inducers of Regulated Cell Death Mechanisms. *Chem. Rev.* **2023**, *123* (16), 10135−10155.

(10) Yin, H.; Stephenson, M.; Gibson, J.; Sampson, E.; Shi, G.; Sainuddin, T.; Monro, S.; McFarland, S. A. In Vitro Multiwavelength PDT with 3IL States: Teaching Old Molecules New Tricks. *Inorg. Chem.* **2014**, *53* (9), 4548−4559.

(11) Gunaydin, G.; Gedik, M. E.; Ayan, S. Photodynamic Therapy-Current Limitations and Novel Approaches. *Front. Chem.* **2021**, *9*, No. 691697.

(12) Correia, J. H.; Rodrigues, J. A.; Pimenta, S.; Dong, T.; Yang, Z. Photodynamic Therapy Review: Principles, Photosensitizers, Applications, and Future Directions. *Pharmaceutics* **2021**, *13* (9), No. 1332.

(13) Wu, Y.; Li, S.; Chen, Y.; He, W.; Guo, Z. Recent advances in noble metal complex based photodynamic therapy. *Chem. Sci.* **2022**, *13* (18), 5085−5106.

(14) Juarranz, Á.; Jaén, P.; Sanz-Rodríguez, F.; Cuevas, J.; González, S. Photodynamic therapy of cancer. Basic principles and applications. *Clin. Transl. Oncol.* **2008**, *10* (3), 148−154.
(15) Simões, J. C. S.; Sarpaki, S.; Papadimitroulas, P.; Therrien, B.; Loudos, G. Conjugated Photosensitizers for Imaging and PDT in Cancer Research. *J. Med. Chem.* **2020**, *63* (23), 14119−14150.
(16) Sun, B.; Bte Rahmat, J. N.; Zhang, Y. Advanced techniques for performing photodynamic therapy in deep-seated tissues. *Biomaterials* **2022**, *291*, No. 121875.
(17) Yoon, I.; Li, J. Z.; Shim, Y. K. Advance in photosensitizers and light delivery for photodynamic therapy. *Clinical Endoscopy* **2013**, *46* (1), 7−23.
(18) Dąbrowski, J. M.; Pucelik, B.; Regiel-Futyra, A.; Brindell, M.; Mazuryk, O.; Kyzioł, A.; Stochel, G.; Macyk, W.; Arnaut, L. G. Engineering of relevant photodynamic processes through structural modifications of metallotetrapyrrolic photosensitizers. *Coord. Chem. Rev.* **2016**, *325*, 67−101.
(19) Otvagin, V. F.; Kuzmina, N. S.; Kudriashova, E. S.; Nyuchev, A. V.; Gavryushin, A. E.; Fedorov, A. Y. Conjugates of Porphyrinoid-Based Photosensitizers with Cytotoxic Drugs: Current Progress and Future Directions toward Selective Photodynamic Therapy. *J. Med. Chem.* **2022**, *65* (3), 1695−1734.
(20) Xue, Q.; Zhang, J.; Jiao, J.; Qin, W.; Yang, X. Photodynamic therapy for prostate cancer: Recent advances, challenges and opportunities. *Front. Oncol.* **2022**, *12*, No. 980239.
(21) Mukherjee, R. A Comprehensive Review for Ruthenium(II) Complexes in Photodynamic Therapy. *Asian J. Chem.* **2023**, *35* (11), 2595−2602.
(22) Pozza, M. D.; Mesdom, P.; Abdullrahman, A.; Otoya, T. D. P.; Arnoux, P.; Frochot, C.; Niogret, G.; Saubamea, B.; Burckel, P.; Hall, J. P.; Hollenstein, M.; Cardin, C. J.; Gasser, G. Increasing the pi-Expansive Ligands in Ruthenium(II) Polypyridyl Complexes: Synthesis, Characterization, and Biological Evaluation for Photodynamic Therapy Applications. *Inorg. Chem.* **2023**, *62* (45), 18510−18523.
(23) Monro, S.; Colon, K. L.; Yin, H.; Roque, J., 3rd; Konda, P.; Gujar, S.; Thummel, R. P.; Lilge, L.; Cameron, C. G.; McFarland, S. A. Transition Metal Complexes and Photodynamic Therapy from a Tumor-Centered Approach: Challenges, Opportunities, and Highlights from the Development of TLD1433. *Chem. Rev.* **2019**, *119* (2), 797−828.
(24) Gianferrara, T.; Bergamo, A.; Bratsos, I.; Milani, B.; Spagnul, C.; Sava, G.; Alessio, E. Ruthenium−Porphyrin Conjugates with Cytotoxic and Phototoxic Antitumor Activity. *J. Med. Chem.* **2010**, *53* (12), 4678−4690.
(25) Vizzotto, B. S.; Dias, R. S.; Iglesias, B. A.; Krause, L. F.; Viana, A. R.; Schuch, A. P. DNA photocleavage and melanoma cells cytotoxicity induced by a meso-tetra-ruthenated porphyrin under visible light irradiation. *J. Photochem. Photobiol., B* **2020**, *209*, No. 111922.
(26) Ge, J.; Lan, M.; Zhou, B.; Liu, W.; Guo, L.; Wang, H.; Jia, Q.; Niu, G.; Huang, X.; Zhou, H.; Meng, X.; Wang, P.; Lee, C.-S.; Zhang, W.; Han, X. A graphene quantum dot photodynamic therapy agent with high singlet oxygen generation. *Nat. Commun.* **2014**, *5* (1), No. 4596.
(27) Amselem, L.; Monés, J. M.; Arias, L. Photosensitizers and Photodynamic Therapy: Verteporfin. In *Retinal Pharmacotherapy*; Nguyen, Q. D.; Rodrigues, E. B.; Farah, M. E.; Mieler, W. F., Eds.; W.B. Saunders, 2010; Chapter 43, pp 297−305.
(28) Gibault, F.; Bailly, F.; Corvaisier, M.; Coevoet, M.; Huet, G.; Melnyk, P.; Cotelle, P. Molecular Features of the YAP Inhibitor Verteporfin: Synthesis of Hexasubstituted Dipyrrins as Potential Inhibitors of YAP/TAZ, the Downstream Effectors of the Hippo Pathway. *ChemMedChem* **2017**, *12* (12), 954−961.
(29) Houle, J. M.; Strong, H. A. Duration of skin photosensitivity and incidence of photosensitivity reactions after administration of verteporfin. *Retina* **2002**, *22* (6), 691−697.
(30) Sung, H.; Ferlay, J.; Siegel, R. L.; Laversanne, M.; Soerjomataram, I.; Jemal, A.; Bray, F. Global Cancer Statistics 2020: GLOBOCAN Estimates of Incidence and Mortality Worldwide for 36 Cancers in 185 Countries. *Ca-Cancer J. Clin.* **2021**, *71* (3), 209−249.
(31) Mihmanli, M.; Ilhan, E.; Idiz, U. O.; Alemdar, A.; Demir, U. Recent developments and innovations in gastric cancer. *World J. Gastroenterol.* **2016**, *22* (17), 4307−4320.
(32) Han, K. H.; Choi, Y. J.; Il Kim, T.; Park, N. H.; Han, K.-d.; Lee, D. H. Association between glycemic status and the risk of gastric cancer in pre/peri-and postmenopausal women: A nationwide cohort study. *Ann. Epidemiol.* **2024**, *94*, 106−112.
(33) Li, Z.; Shu, X.; Liu, X.; Li, Q.; Hu, Y.; Jia, B.; Song, M. Cellular and Molecular Mechanisms of Chemoresistance for Gastric Cancer. *Int. J. Gen. Med.* **2024**, *17*, 3779−3788.
(34) Blanchet, A.; Bourgmayer, A.; Kurtz, J.-E.; Mellitzer, G.; Gaiddon, C. Isoforms of the p53 Family and Gastric Cancer: A Ménage à Trois for an Unfinished Affair. *Cancers* **2021**, *13* (4), No. 916.
(35) Vidimar, V.; Meng, X.; Klajner, M.; Licona, C.; Fetzer, L.; Harlepp, S.; Hebraud, P.; Sidhoum, M.; Sirlin, C.; Loeffler, J. P.; Mellitzer, G.; Sava, G.; Pfeffer, M.; Gaiddon, C. Induction of caspase 8 and reactive oxygen species by ruthenium-derived anticancer compounds with improved water solubility and cytotoxicity. *Biochem. Pharmacol.* **2012**, *84* (11), 1428−1436.
(36) Vidimar, V.; Licona, C.; Cerón-Camacho, R.; Guerin, E.; Coliat, P.; Venkatasamy, A.; Ali, M.; Guenot, D.; Le Lagadec, R.; Jung, A. C.; Freund, J.-N.; Pfeffer, M.; Mellitzer, G.; Sava, G.; Gaiddon, C. A redox ruthenium compound directly targets PHD2 and inhibits the HIF1 pathway to reduce tumor angiogenesis independently of p53. *Cancer Lett.* **2019**, *440*−*441*, 145−155.
(37) Riegel, G.; Orvain, C.; Recberlik, S.; Spaety, M. E.; Poschet, G.; Venkatasamy, A.; Yamamoto, M.; Nomura, S.; Tsukamoto, T.; Masson, M.; Gross, I.; Le Lagadec, R.; Mellitzer, G.; Gaiddon, C. The unfolded protein response-glutathione metabolism axis: A novel target of a cycloruthenated complexes bypassing tumor resistance mechanisms. *Cancer Lett.* **2024**, *585*, No. 216671.
(38) Miyata, K.; Yasuda, S.; Masuya, T.; Ito, S.; Kinoshita, Y.; Tamiaki, H.; Oba, T. Facile iodination of the vinyl groups in protoporphyrin IX dimethyl ester and subsequent transformation of the iodinated moieties. *Tetrahedron* **2018**, *74* (27), 3707−3711.
(39) Morgan, A. R.; Kohli, D. H. Diels-alder reactions of protoporphyrin IX dimethyl ester. *Tetrahedron Lett.* **1995**, *36* (42), 7603−7606.
(40) de Oliveira, K. T.; Silva, A. M. S.; Tomé, A. C.; Neves, M. G. P. M. S.; Neri, C. R.; Garcia, V. S.; Serra, O. A.; Iamamoto, Y.; Cavaleiro, J. A. S. Synthesis of new amphiphilic chlorin derivatives from protoporphyrin-IX dimethyl ester. *Tetrahedron* **2008**, *64* (37), 8709−8715.
(41) Rebouças, J. S.; James, B. R. Ruthenium(II) complexes of meso-tetrakis(4-cyanophenyl)porphyrin. *Inorg. Chem. Commun.* **2013**, *30*, 49−52.
(42) Chow, B. C.; Cohen, I. A. Derivatives of tetraphenylporphineruthenium (II). *Bioinorg. Chem.* **1971**, *1* (1), 57−63.
(43) Thandiayyakone, V.; Murugan, A.; Ravikumar, C. R.; Rajkumar, T.; Arasu, P. T.; Yadav, H. S.; Kotteeswaran, P. Studies on redox and axial ligand properties of Meso-Mn(III) porphyrin by cyclic voltammetry and UV−Visible spectrophotometry. *Mater. Today: Proc.* **2021**, *47*, 933−937.
(44) Dar, U. A.; Shah, S. A. UV−visible and fluorescence spectroscopic assessment of meso-tetrakis-(4-halophenyl) porphyrin; H2TXPP (X = F, Cl, Br, I) in THF and THF-water system: Effect of pH and aggregation behaviour. *Spectrochim. Acta, Part A* **2020**, *240*, No. 118570.
(45) Nas, A.; Fandaklı, S.; Kantekin, H.; Demirbaş, A.; Durmuş, M. Novel organosoluble metal-free and metallophthalocyanines bearing triazole moieties: Microwave assisted synthesis and determination of photophysical and photochemical properties. *Dyes Pigm.* **2012**, *95* (1), 8−17.
(46) Linares, I. A. P.; de Oliveira, K. T.; Perussi, J. R. Chlorin derivatives sterically-prevented from self-aggregation with high

https://doi.org/10.1021/acs.inorgchem.5c00896
Inorg. Chem. 2025, 64, 9684−9702

antitumor activity for photodynamic therapy. *Dyes Pigm.* **2017**, *145*, 518−527.
(47) Spiller, W.; Kliesch, H.; Wöhrle, D.; Hackbarth, S.; Röder, B.; Schnurpfeil, G. Singlet oxygen quantum yields of different photosensitizers in polar solvents and micellar solutions. *J. Porphyrins Phthalocyanines* **1998**, *2* (2), 145−158.
(48) Pan, J.; Jiang, L.; Chan, C.-F.; Tsoi, T.-H.; Shiu, K.-K.; Kwong, D. W. J.; Wong, W.-T.; Wong, W.-K.; Wong, K.-L. Excitation energy transfer in ruthenium (II)-porphyrin conjugates led to enhanced emission quantum yield and $^1O_2$ generation. *J. Lumin.* **2017**, *184*, 89−95.
(49) McCarthy, J. R.; Weissleder, R. Model Systems for Fluorescence and Singlet Oxygen Quenching by Metalloporphyrins. *ChemMedChem* **2007**, *2* (3), 360−365.
(50) Mani, A.; Feng, T.; Gandioso, A.; Vinck, R.; Notaro, A.; Gourdon, L.; Burckel, P.; Saubaméa, B.; Blacque, O.; Cariou, K.; Belgaied, J.-E.; Chao, H.; Gasser, G. Structurally Simple Osmium(II) Polypyridyl Complexes as Photosensitizers for Photodynamic Therapy in the Near Infrared. *Angew. Chem., Int. Ed.* **2023**, *62* (20), No. e202218347.
(51) Rovira, A.; Ortega-Forte, E.; Hally, C.; Jordà-Redondo, M.; Abad-Montero, D.; Vigueras, G.; Martínez, J. I.; Bosch, M.; Nonell, S.; Ruiz, J.; Marchán, V. Exploring Structure−Activity Relationships in Photodynamic Therapy Anticancer Agents Based on Ir(III)-COUPY Conjugates. *J. Med. Chem.* **2023**, *66* (12), 7849−7867.
(52) Buettner, G. R. Spin Trapping: ESR parameters of spin adducts 1474 1528V. *Free Radical Biol. Med.* **1987**, *3* (4), 259−303.
(53) Brahmi, J.; Nasri, S.; Saidi, H.; Nasri, H.; Aouadi, K. Synthesis of New Porphyrin Complexes: Evaluations on Optical, Electrochemical, Electronic Properties and Application as an Optical Sensor. *ChemistrySelect* **2019**, *4* (4), 1350−1359.
(54) Xu, S.; Yuan, Y.; Cai, X.; Zhang, C.-J.; Hu, F.; Liang, J.; Zhang, G.; Zhang, D.; Liu, B. Tuning the singlet-triplet energy gap: a unique approach to efficient photosensitizers with aggregation-induced emission (AIE) characteristics. *Chem. Sci.* **2015**, *6* (10), 5824−5830.
(55) Fukuzumi, S.; Ohkubo, K.; Zheng, X.; Chen, Y.; Pandey, R. K.; Zhan, R.; Kadish, K. M. Metal Bacteriochlorins Which Act as Dual Singlet Oxygen and Superoxide Generators. *J. Phys. Chem. B* **2008**, *112* (9), 2738−2746.
(56) Daina, A.; Michielin, O.; Zoete, V. iLOGP: A Simple, Robust, and Efficient Description of n-Octanol/Water Partition Coefficient for Drug Design Using the GB/SA Approach. *J. Chem. Inf. Model.* **2014**, *54* (12), 3284−3301.
(57) Stephan, K.; Saab, J.; Mokbel, I.; Goutaudier, C.; Ferrigno, R. Continuous-flow microfluidic method for octanol-water partition coefficient measurement. *Fluid Phase Equilib.* **2014**, *380*, 116−120.
(58) Kim, K.; Park, H.; Lim, K.-M. Phototoxicity: Its Mechanism and Animal Alternative Test Methods. *Toxicol. Res.* **2015**, *31* (2), 97−104.
(59) Heinemann, F.; Karges, J.; Gasser, G. Critical Overview of the Use of Ru(II) Polypyridyl Complexes as Photosensitizers in One-Photon and Two-Photon Photodynamic Therapy. *Acc. Chem. Res.* **2017**, *50* (11), 2727−2736.
(60) Liu, X.; Li, G.; Xie, M.; Guo, S.; Zhao, W.; Li, F.; Liu, S.; Zhao, Q. Rational design of type I photosensitizers based on Ru(II) complexes for effective photodynamic therapy under hypoxia. *Dalton Trans.* **2020**, *49* (32), 11192−11200.
(61) Mishchenko, T.; Balalaeva, I.; Gorokhova, A.; Vedunova, M.; Krysko, D. V. Which cell death modality wins the contest for photodynamic therapy of cancer? *Cell Death Dis.* **2022**, *13* (5), No. 455.
(62) Ha, J.-H.; Kim, Y.-J. Photodynamic and Cold Atmospheric Plasma Combination Therapy Using Polymeric Nanoparticles for the Synergistic Treatment of Cervical Cancer. *Int. J. Mol. Sci.* **2021**, *22* (3), No. 1172.
(63) Brabec, V.; Kasparkova, J. Ruthenium coordination compounds of biological and biomedical significance. DNA binding agents. *Coord. Chem. Rev.* **2018**, *376*, 75−94.
(64) Sudhindra, P.; Sharma, S. A.; Roy, N.; Moharana, P.; Paira, P. Recent advances in cytotoxicity, cellular uptake and mechanism of action of ruthenium metallodrugs: A review. *Polyhedron* **2020**, *192*, No. 114827.
(65) Dorairaj, D. P.; Haribabu, J.; Dharmasivam, M.; Malekshah, R. E.; Subarkhan, M. K. M.; Echeverria, C.; Karvembu, R. Ru(II)-p-Cymene Complexes of Furoylthiourea Ligands for Anticancer Applications against Breast Cancer Cells. *Inorg. Chem.* **2023**, *62* (30), 11761−11774.
(66) Xu, Z.; Li, C.; Zhou, Q.; Deng, Z.; Tong, Z.; Tse, M.-K.; Zhu, G. Synthesis, Cytotoxicity, and Mechanistic Investigation of Platinum-(IV) Anticancer Complexes Conjugated with Poly(ADP-ribose) Polymerase Inhibitors. *Inorg. Chem.* **2019**, *58* (23), 16279−16291.
(67) Chen, X.; Mao, J.; Zhou, L.; Jiang, W.; Li, Z.; Li, Y.; Chen, S.; Tan, G.; Xie, Y.; Wang, C.; Sun, J. Reducing PKCδ inhibits tumor growth through growth hormone by inhibiting PKA/CREB/ERK signaling pathway in pituitary adenoma. *Sci. Rep.* **2025**, *15* (1), No. 11461.
(68) Devarajan, E.; Sahin, A. A.; Chen, J. S.; Krishnamurthy, R. R.; Aggarwal, N.; Brun, A.-M.; Sapino, A.; Zhang, F.; Sharma, D.; Yang, X.-H.; Tora, A. D.; Mehta, K. Down-regulation of caspase 3 in breast cancer: a possible mechanism for chemoresistance. *Oncogene* **2002**, *21* (57), 8843−8851.
(69) Ding, M.; Ma, C.; Lin, Y.; Fang, H.; Xu, Y.; Wang, S.; Chen, Y.; Zhou, J.; Gao, H.; Shan, Y.; Yang, L.; Sun, H.; Tang, Y.; Wu, X.; Zhu, L.; Zheng, L.; Assaraf, Y. G.; Zhou, B.-B. S.; Gu, S.; Li, H. Therapeutic targeting de novo purine biosynthesis driven by β-catenin-dependent PPAT upregulation in hepatoblastoma. *Cell Death Dis.* **2025**, *16* (1), No. 179.
(70) Pan, M.; Zhang, Y.; Wright, W. C.; Liu, X.; Passaia, B.; Currier, D.; Low, J.; Chapple, R. H.; Steele, J. A.; Connelly, J. P.; Ju, B.; Plyler, E.; Lu, M.; Loughran, A. J.; Yang, L.; Abraham, B. J.; Pruett-Miller, S. M.; Freeman, B.; Campbell, G. E.; Dyer, M. A.; Chen, T.; Stewart, E.; Koo, S.; Sheppard, H.; et al. Bone morphogenetic protein (BMP) signaling determines neuroblastoma cell fate and sensitivity to retinoic acid. *Nat. Commun.* **2025**, *16* (1), No. 2036.
(71) Fang, J.; Huang, X.; Yang, Y.; Wang, X.; Liang, X.; Liu, J. Berberine-photodynamic induced apoptosis by activating endoplasmic reticulum stress-autophagy pathway involving CHOP in human malignant melanoma cells. *Biochem. Biophys. Res. Commun.* **2021**, *552*, 183−190.
(72) Lee, Y.-S.; Lee, D.-H.; Choudry, H. A.; Bartlett, D. L.; Lee, Y. J. Ferroptosis-Induced Endoplasmic Reticulum Stress: Cross-talk between Ferroptosis and Apoptosis. *Mol. Cancer Res.* **2018**, *16* (7), 1073−1076.
(73) Ochoa, C. D.; Wu, R. F.; Terada, L. S. ROS signaling and ER stress in cardiovascular disease. *Mol. Aspects Med.* **2018**, *63*, 18−29.
(74) Zhao, T.; Wu, K.; Hogstrand, C.; Xu, Y.-H.; Chen, G.-H.; Wei, C.-C.; Luo, Z. Lipophagy mediated carbohydrate-induced changes of lipid metabolism via oxidative stress, endoplasmic reticulum (ER) stress and ChREBP/PPARγ pathways. *Cell. Mol. Life Sci.* **2020**, *77* (10), 1987−2003.
(75) Verfaillie, T.; Salazar, M.; Velasco, G.; Agostinis, P. Linking ER Stress to Autophagy: Potential Implications for Cancer Therapy. *Int. J. Cell Biol.* **2010**, *2010* (1), No. 930509.
(76) Song, S.; Tan, J.; Miao, Y.; Li, M.; Zhang, Q. Crosstalk of autophagy and apoptosis: Involvement of the dual role of autophagy under ER stress. *J. Cell. Physiol.* **2017**, *232* (11), 2977−2984.
(77) Kania, E.; Pająk, B.; Orzechowski, A. Calcium Homeostasis and ER Stress in Control of Autophagy in Cancer Cells. *BioMed Res. Int.* **2015**, *2015* (1), No. 352794.
(78) Luo, M.; Li, H.; Han, D.; Yang, K.; Kang, L. Inhibition of autophagy enhances apoptosis induced by Ce6-photodynamic therapy in human colon cancer cells. *Photodiagn. Photodyn. Ther.* **2021**, *36*, No. 102605.
(79) Rouschop, K.; Bradly, G. W. Regulation of Autophagy Through Multiple Independent Hypoxic Signaling Pathways. *Curr. Mol. Med.* **2009**, *9* (4), 417−424.

https://doi.org/10.1021/acs.inorgchem.5c00896
Inorg. Chem. 2025, 64, 9684−9702

(80) Ouyang, G.; Xiong, L.; Liu, Z.; Lam, B.; Bui, B.; Ma, L.; Chen, X.; Zhou, P.; Wang, K.; Zhang, Z.; Huang, H.; Miao, X.; Chen, W.; Wen, Y. Inhibition of autophagy potentiates the apoptosis-inducing effects of photodynamic therapy on human colon cancer cells. *Photodiagn. Photodyn. Ther.* **2018**, *21*, 396−403.
(81) Sun, Y.; Chen, P.; Zhai, B.; Zhang, M.; Xiang, Y.; Fang, J.; Xu, S.; Gao, Y.; Chen, X.; Sui, X.; Li, G. The emerging role of ferroptosis in inflammation. *Biomed. Pharmacother.* **2020**, *127*, No. 110108.
(82) Kajarabille, N.; Latunde-Dada, G. O. Programmed Cell-Death by Ferroptosis: Antioxidants as Mitigators. *Int. J. Mol. Sci.* **2019**, *20* (19), No. 4968.
(83) Friedmann Angeli, J. P.; Krysko, D. V.; Conrad, M. Ferroptosis at the crossroads of cancer-acquired drug resistance and immune evasion. *Nat. Rev. Cancer* **2019**, *19* (7), 405−414.
(84) Gurram, B.; Zhang, S.; Li, M.; Li, H.; Xie, Y.; Cui, H.; Du, J.; Fan, J.; Wang, J.; Peng, X. Celecoxib Conjugated Fluorescent Probe for Identification and Discrimination of Cyclooxygenase-2 Enzyme in Cancer Cells. *Anal. Chem.* **2018**, *90* (8), 5187−5193.
(85) Hashemi Goradel, N.; Najafi, M.; Salehi, E.; Farhood, B.; Mortezaee, K. Cyclooxygenase-2 in cancer: A review. *J. Cell. Physiol.* **2019**, *234* (5), 5683−5699.
(86) Fauré, M.; Saccavini, C.; Lavigne, G. New insight into a convenient base-promoted synthesis of $Ru_3(CO)_{12}$. *Chem. Commun.* **2003**, No. 13, 1578−1579.
(87) *SAINT*; Bruker AXS Inc.: Madison, Wisconsin, USA, 2012.
(88) *APEX2*; Bruker AXS Inc.: Madison, Wisconsin, USA, 2012.
(89) de Assis, F. F.; de Souza, J. M.; Assis, B. H. K.; Brocksom, T. J.; de Oliveira, K. T. Synthesis and photophysical studies of a chlorin sterically designed to prevent self-aggregation. *Dyes Pigm.* **2013**, *98* (1), 153−159.
(90) Siahcheshm, P.; Heiden, P. High quantum yield carbon quantum dots as selective fluorescent turn-off probes for dual detection of Fe^{2+}/Fe^{3+} ions. *J. Photochem. Photobiol., A* **2023**, *435*, No. 114284.
(91) Li, Y.; Liu, Y.; Shang, X.; Chao, D.; Zhou, L.; Zhang, H. Highly sensitive and selective detection of Fe^{3+} by utilizing carbon quantum dots as fluorescent probes. *Chem. Phys. Lett.* **2018**, *705*, 1−6.
(92) Seotsanyana-Mokhosi, I.; Kuznetsova, N.; Nyokong, T. Photochemical studies of tetra-2,3-pyridinoporphyrazines. *J. Photochem. Photobiol., A* **2001**, *140* (3), 215−222.
(93) Swavey, S.; Quentel, A.; Grzesiak, M.; Hawkins, C.; Vidi, P.-A. Efficient light-induced reactive oxygen species production from a far-red ER-targeting BODIPY dye. *RSC Adv.* **2024**, *14* (52), 38796−38805.
(94) Benson, S.; de Moliner, F.; Fernandez, A.; Kuru, E.; Asiimwe, N. L.; Lee, J.-S.; Hamilton, L.; Sieger, D.; Bravo, I. R.; Elliot, A. M.; Feng, Y.; Vendrell, M. Photoactivatable metabolic warheads enable precise and safe ablation of target cells in vivo. *Nat. Commun.* **2021**, *12* (1), No. 2369.
(95) Nardi, G.; Manet, I.; Monti, S.; Miranda, M. A.; Lhiaubet-Vallet, V. Scope and limitations of the TEMPO/EPR method for singlet oxygen detection: the misleading role of electron transfer. *Free Radical Biol. Med.* **2014**, *77*, 64−70.
(96) Andrés, A.; Rosés, M.; Ràfols, C.; Bosch, E.; Espinosa, S.; Segarra, V.; Huerta, J. M. Setup and validation of shake-flask procedures for the determination of partition coefficients (logD) from low drug amounts. *Eur. J. Pharm. Sci.* **2015**, *76*, 181−191.
(97) Ballester, F. J.; Ortega, E.; Bautista, D.; Santana, M. D.; Ruiz, J. Ru(II) photosensitizers competent for hypoxic cancers via green light activation. *Chem. Commun.* **2020**, *56* (71), 10301−10304.
(98) Sun, J.; Wang, Y.; Du, Y.; Zhang, W.; Liu, Z.; Bai, J.; Cui, G.; Du, Z. Involvement of the JNK/HO-1/FTH1 signaling pathway in nanoplastic-induced inflammation and ferroptosis of BV2 microglia cells. *Int. J. Mol. Med.* **2023**, *52* (1), No. 61.
(99) Schneider, C. A.; Rasband, W. S.; Eliceiri, K. W. NIH Image to ImageJ: 25 years of image analysis. *Nat. Methods* **2012**, *9* (7), 671−675.

https://doi.org/10.1021/acs.inorgchem.5c00896
Inorg. Chem. 2025, 64, 9684−9702